To the Graduate Council:

I am submitting herewith a thesis written by Michelle Yvonne Vella entitled "An Experimental Study: Using Honeycomb to Reduce Secondary Flows in Curved Ducts." I have examined the final paper copy of this thesis for form and content and recommend that it be accepted in partial fulfillment of the requirements for the degree of Master of Science, with a major in Aerospace Engineering.

Ahmad D. Vakili, Major Professor

We have read this thesis and recommend its acceptance:

Charles C. Limbaugh

Ralph D. Kimberlin

Acceptance for the Council:

Vice Provost and Dean of Graduate Studies

An Experimental Study: Using Honeycomb to Reduce Secondary Flows in Curved Ducts

A Thesis
Presented for the
Master of Science
Degree
The University of Tennessee, Knoxville

Michelle Yvonne Vella
August 2003

Thesis
2003
.V45

Acknowledgements

I would like to thank my advisor, Dr Vakili, his guidance, motivation, and patience were instrumental in the success of this project. I also want to thank the other members of my committee, Dr Limbaugh and Dr Kimberlin for their time and suggestions. I would like to acknowledge Jim Goodman, Keith Walker, and Chris Armstrong at the Propulsion Lab; their hard work and expertise throughout my experimental process and their continual support when I needed to conduct more experiments are greatly appreciated. My thanks and appreciation are also due to Linda Engels for her expertise in graphics and Brenda Brooks for her help in obtaining the many papers that I requested; their kindness and assistance are gratefully acknowledged. I want to give a special thanks to Abraham Meganathan for his help in conducting the Particle Imagining Velocimetry experiments. I want to thank my Canadian colleague Jeff Daly and his family for their friendship and support.

Most importantly I would like to acknowledge my friends and family for their love and support. In particular my parents, Yvonne and Charles, they have supported and believed in me, in all my endeavors-I am very grateful. To my best friend Angela, thank-you for reading my material but most importantly for your friendship. And to my fiancé Scot, my biggest cheerleader, thank-you for everything-especially your love and encouragement-you are truly wonderful.

Abstract

This experimental study evaluated the effectiveness of using honeycomb to improve flow quality by reducing secondary flow in curved ducts. An experimental setup that consisted of two 90° elbows joined by a 6-inch straight connector duct was used. Traditional solid honeycomb and honeycombs of varying porosity (20%, 30%, and 40%) were installed at either of two locations in the flow: after the 1st elbow or after the 2nd elbow. Surface oil flow visualization, pressure measurements, and Particle Imaging Velocimetry (PIV) were used to determine the improvement in flow quality with the honeycombs installed and to determine if the secondary flows in the exit duct diminish within a shorter distance downstream compared to the baseline flow. Surface oil flow visualization provided a qualitative representation of flow behavior in the exit duct; analysis of pressure measurements provided insight on how the flow traveling through the elbows and into the exit duct was affected by different free-stream velocities; and PIV described the vorticity contours in the exit duct.

The experimental results revealed that the honeycombs significantly improve the flow quality in the exit duct by reducing secondary flow generated by the elbows. It was also revealed that the porous-cell honeycombs were able to further eliminate more of the non-uniformities in the flow than the traditional solid honeycomb. The solid and porous-cell honeycombs helped to generate a more uniform flow within a shorter distance downstream in the exit duct than the baseline flow.

Table of Contents

List of Figures

Nomenclature

De	Dean Number
Re	Reynolds Number
D_p	Diameter of the Duct
r	Radius of the Duct
R	Radius of Curvature of Elbow
L	Total Length of Duct
K, C_p	Pressure Loss Coefficient, Pressure Coefficient
q	Dynamic Pressure
ρ	Fluid Density
μ	Fluid Viscosity
V	Fluid Velocity
δ	Boundary Layer Height
x	Distance
Re_x	Reynolds Number Based on Distance x
θ_1	Angle of 1st Elbow
θ_2	Angle of 2nd Elbow
ε	Surface Roughness of Duct
P_s	Static Pressure on Duct Wall
P_{ref}	Reference Static Pressure
ΔP	Change in Static Pressure
U_∞	Free-Stream Velocity
$\bar{U}$	Mean Velocity

Δx	Downstream Distance of Honeycomb
l_{hc}	Length of Honeycomb Cell
l_{pa}	Length of Porous Area
t	Diameter of Honeycomb Cell
A_p	Porous Area of Honeycomb Cell
A_t	Total Area of Honeycomb Cell
f	Turbulence Reduction Factor
f1	Axial Turbulence Reduction Factor
f2	Lateral Turbulence Reduction Factor
F	Generic Variable
f	Functional Relation

Chapter 1

Introduction

Flow in elbows and s-shaped ducts have been studied for a number of years [1]. It is known that flow in curved pipes generate secondary flows. The larger centrifugal force that acts on the higher velocity flow near the centerline compared to the slower velocity flow near the wall, causes the secondary flow [1]. The fluid at the center moves outward, while the fluid at the wall is pushed inward.

Considerable research has been undertaken to try to eliminate or reduce secondary flows and to reduce losses in the duct generated by the curves. Much of the research that has been undertaken involves aerodynamic applications such as wind and water tunnels to help improve the flow in the test section [2,3]; however, this research is also becoming more important in other applications such as flight and flow metering. Flight applications include inlets and ducts leading to the engine of high performance aircraft. It is desirable to have ducts that are short and s-shaped to help decrease size and weight and to achieve high total pressure recovery flow. In industrial applications, flow metering is very important; the use of long length pipes is often required to ensure that uniformity of flow is achieved [4]. Improving the efficiency of these systems by decreasing pipe length is essential.

Control devices such as vortex generators, honeycombs, and screens are a few of the methods used to make flow more efficient but these methods are not capable of significantly improving efficiency by reducing pipe length.

Vakili [5] has developed a new flow control concept that uses porous-cell honeycomb with potential for improving flow quality. The concept has been tested in a straight duct wind tunnel test section and the porous-cell honeycomb was compared to a solid honeycomb. Results indicate that the porous-cell honeycomb is more effective than the solid honeycomb at reducing large-scale turbulence. By applying this concept to a curved duct the potential exists to improve flow quality by reducing secondary flows, as well as reducing the length of duct required after the device to establish uniform flow.

This thesis study is an experimental investigation of the effectiveness of using honeycombs as a passive flow control device to improve flow quality in curved ducts by reducing secondary flows. The thesis is that porous-cell honeycomb will improve flow quality in the exit section of a duct by allowing the disturbances in the flow field to be reduced as it moves between adjacent cells in the honeycomb.

A relatively simple apparatus, Figure 1-1, was developed to study the duct flow. The apparatus consisted of a straight inlet duct leading to two 90° elbows, joined by a 6-inch straight connector duct. The elbows created an offset in the flow, which is typical in many industrial applications. The straight inlet section connected to a pressure apparatus, which supplied the flow. Downstream of the 2nd elbow was a straight exit duct, whose main purpose was to ensure that no upstream effects were generated by the flow exiting to the atmosphere. The effectiveness of the honeycomb was evaluated by utilizing the experimental techniques of surface oil flow visualization, pressure transducer measurements, and Particle Imaging Velocimetry (PIV) and comparing results of the porous-cell honeycomb to that of a baseline flow (no flow control device) and a solid honeycomb.

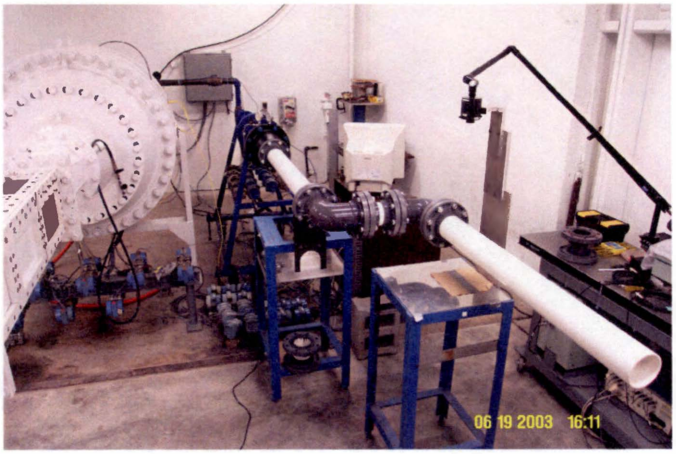

Figure 1-1. Duct Setup

Chapter 2

Background and Literature Review

Pipe flow and its applications have been studied for many years [1]. Ways to improve the flow inside ducts by reducing turbulence and flow separation, especially in areas of the duct where curves, fittings, and other components are located are of particular importance.

Flow meters, used to measure the flow through pipes, are significantly affected by their installation conditions. Fluid flow and mechanical devices also affect flow meters [4]. Various ways fluid flow affects flow meters include but are not limited to the presence of swirl, non-uniform or non-axial flow, as well as poor flow profiles. Mechanical effects include pipe fittings that are too close to the location of the flow meter. The user of the flow meter must ensure that the meter is installed correctly and that a good operating environment exists; as a result, long length pipe work upstream and downstream of the meter is often required [6].

Flow in curved ducts results in the generation of significant flow disturbances and secondary flows. The secondary flow in curved ducts exists because the high velocity flow near the centerline is acted upon by a larger centrifugal force than the slower velocity flow near the wall [1]. The higher velocity flow moves outward, forcing the fluid in the boundary layer at the outer wall towards the inner wall. As a result, flow is continually retarded and unable to overcome the adverse pressure fields. As the flow moves from a straight duct to a curved duct, the static pressure on the inside bend decreases while the static pressure on the outer bend increases, resulting in a thickening of the boundary layer [7]. At the same time, flow separation in curved ducts occurs on the inside bend and continues downstream. The extent of flow separation in the bend affects the flow's uniformity in the exit duct, as discussed later. Significant loss of energy results when the flow encounters a bend or a curve. The energy expended is that used by the flow trying to resume a more uniform path [8]. Figure 2-1 [1] illustrates the motion of the fluid when it encounters a curve in the duct. Figure 2-2 [1] illustrates the velocity profile as the flow leaves a curved duct. The flow is no longer uniform.

The influence of the curvature of the duct is characterized by the Dean number [1], a dimensionless parameter,

$$De := \frac{1}{2} \cdot Re \cdot \sqrt{\frac{r}{R}}$$

Where Re is the Reynolds number, r is the radius of duct elbow, and R is the radius of curvature of the elbow.

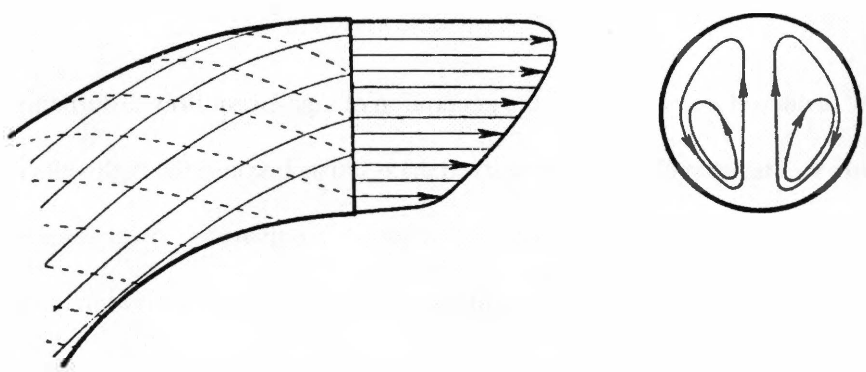

Figure 2-1. Fluid Motion in a Curved Duct

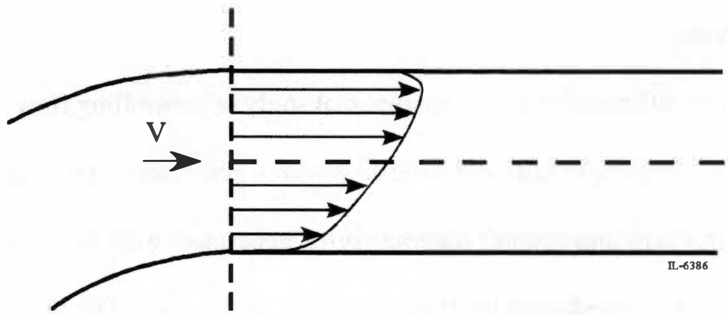

Figure 2-2. Velocity Profile After a Bend

Flow control in curved ducts is very important to help improve flow performance. Flow control devices and turbulence reducers can help the duct flow become more efficient. Research has been conducted into flow control in s-ducts, particularly diffusing s-ducts by means of active and passive flow control devices. S-ducts have 2 consecutive elbows that create an offset in the flow and diffusing s-ducts are only special cases of the constant area s-duct, where the exit of the duct is larger than the duct inlet. The purpose of the diffusing s-ducts is to decelerate the flow. Active flow control devices aid the retarding boundary layer by supplementing it with high-energy fluid such as blowing or removing the retarding flow with devices such as suction [9]. These devices are applied to the flow only when necessary. Passive flow control devices are surface discontinuities installed in the flow to enhance natural flow mixing and to energize the retarding flow so that it is able to overcome adverse pressure fields [9]. Passive flow control devices are used in specific design conditions and may be detrimental to the flow; therefore, caution must be taken in evaluating their performance. These devices include vortex generators and micro bumps.

Studies using vortex generators, micro bumps, honeycomb and screens, to name a few, have been analyzed to try to develop new and improved ways of controlling flow in curved ducts.

Flow Control Devices

Vakili et al. [9] performed an experimental study of controlling flow in a diffusing s-duct by means of flow control rails and wing-like vortex generators. They determined that thicker flow control rails and counter rotating vortex generators were both successful in eliminating or effectively reducing the flow separation in the duct. The flow control rails, however, generated significant disturbances in the flow field that continued into the exit duct, resulting in a large component of secondary flow. They also determined that the vortex generators produced better pressure recovery with reduced secondary flow in the exit duct than the control rails. The control rails actually increased the level of secondary flow from the baseline value.

Reichert et al [10] researched ways to reduce flow distortion (improve flow uniformity) and improve the total pressure recovery in diffusing s-ducts. Reichert utilized tapered-fin type vortex generators in various configurations to help improve the flow. The main goal was to use the vortex generators to control the development of secondary flow. Reichert's team was able to reduce flow distortion by 50% and improve the total pressure recovery by 0.5% [10].

Similarly, Anabtawi et al [11] conducted experiments in diffusing s-ducts with and without passive flow control. They utilized vortex generators as the flow control device. Results indicated that very large vortex generators, heights on the order of the entering boundary layer thickness, were very effective. These vortex generators also improved pressure recovery only slightly but significantly lowered the total pressure distortion.

Jenkins et al [12] performed studies using flow control devices for internal flows. The studies focused on passive micro vortex generators, micro bumps, and piezoelectric synthetic jets to evaluate their flow control characteristics. These devices were evaluated using surface static pressures, flow visualization, and particle imaging velocimetry. Jenkins et al [12] determined that micro vortex generators were effective in controlling the flow through re-energization of boundary layer mixing. The micro bumps did not demonstrate any positive characteristics in improving the flow; and the piezoelectric synthetic jets required enough velocity output to produce vortices so as to penetrate into the flow to be effective [12].

Screens and honeycombs are also used in internal flows. Often they are used in applications such as wind tunnels to improve flow uniformity. Wind tunnel fans, corners, elbows, flow separation, and wind tunnel walls upstream from the working section create eddies, or secondary motions in wind tunnels or any pipe flow. Screens help to reduce the velocity disturbances in a flow that pass through it. In other words, Screens are used to remove (or create) flow non-uniformities and to control turbulence scale and intensity [13]. Screens reduce axial disturbances more than lateral disturbances; since there is a high pressure loss across a screen, axial disturbances in velocity for example, help to distribute the higher velocity regions into the lower velocity regions resulting in a more uniform flow [3]. Honeycombs are used in a similar manner, however honeycombs have a greater effect of establishing a uniform velocity profile and reducing vortices. Honeycombs are essentially flow conditioners that suppress the level of lateral turbulence generated upstream.

Since screens alone are not very effective in removing swirl or large-scale eddy motions, honeycombs and screens are often used in combination and are a very useful method of improving flow control. They are effective turbulence management systems in wind tunnels and are also used as conditioning devices in flow metering applications [13].

Dryden and Schubauer [14] performed tests in a 4-½ foot wind tunnel with screens installed in the settling chamber. They analyzed the use of screens for the reduction of wind tunnel turbulence. From their work it was determined that the effect of a screen in reducing the turbulence of the air stream was dependent upon the pressure drop coefficient, K, of the screen.

K is defined as the pressure loss across the screen divided by the dynamic pressure of the mean flow:

$K = \Delta P/q$

Where: $q = \frac{1}{2} \rho V^2$.

It was also determined that for the same power expenditure, a greater turbulence reduction can be obtained with a number of screens with small K, than with a single screen of coefficient, nK [14].

Their results indicate that the screen smoothes an air stream by decreasing the turbulent motions of larger scale than the mesh size. The screens, at the same time as reducing the level of turbulence, create turbulent motions of a smaller scale. This is beneficial since small-scale turbulence decays more rapidly than large-scale turbulence and as a result, the screens overall effect is a smoothing of the airflow in which both scale and intensity of the turbulence are reduced [14].

As flow travels through a honeycomb section, it is split into a number of parallel pressure driven pipe flows [15]. In pipe flow, there is a pressure difference across the flow; each honeycomb cell then may have a different inlet pressure. The walls of each honeycomb cell help to reduce the lateral disturbances in the flow. If the honeycomb length is long enough, the flow will become fully developed and the boundary layer will become turbulent since the flow entering the honeycomb is turbulent. The turbulence of the pipe flow is reduced, to a scale on the order of approximately the honeycomb cell diameter, when passing through the honeycomb. The smaller scale turbulence and the turbulence generated by the honeycomb dissipate much more quickly than the larger scale turbulence [15].

Lumley [16] performed a study on the passage of a turbulent stream through honeycomb of large length-to-diameter ratio. His analysis detailed that the flow must be a fully developed turbulent flow to achieve a reduction in the lateral velocity components. Lumley's analysis developed conditions to achieve a fully developed turbulent cell flow with the following assumptions: 1. transition occurs at a length Reynolds number of 10^5 and, 2. the diameter Reynolds number is greater than 2000. Under these assumptions, the boundary layer would grow according to the turbulent flat plate boundary layer equation:

$$\delta/x = 0.37Re_x^{-1/5}$$

Fully developed flow occurred at $\delta = D_p/2$.

Lumley developed design charts that enable experimentalists to obtain a rough range of values for honeycomb length-to-diameter ratio in order to achieve a reduction in turbulence.

A study by Loehrke and Nagib [17] studied the control of free-stream turbulence by means of honeycombs. Their aim was to understand how honeycombs functioned and to look at more efficient ways of utilizing them in the control of free stream turbulence. Loehrke and Nagib used varying lengths of honeycomb to examine the reduction of turbulence. Their results illustrate that as cell length increases, the boundary layer is more developed and therefore, the distance between the centerlines of the jets is wider, wider than that it would be with a shorter honeycomb cell length. The larger wake between jets created larger instabilities between adjacent cell flows. The turbulence generated by the shorter honeycomb cells decayed more rapidly than the turbulence generated by the longer honeycomb cells. Loehrke and Nagib also added a fine mesh screen to the exit of their honeycomb. Results indicate that the single fine mesh screen increased the decay rate of the generated turbulence significantly. Their results suggest that to achieve the best reduction in free stream turbulence, honeycombs and screens should be used in combination with the first screen located near the exit plane of the honeycomb a distance of approximately $\Delta x/t<5$. They also suggest that the honeycomb be the shortest length possible, $l_{hc}/t\sim10$.

Farell et al. [13] performed an experimental study of turbulence management in a pipe using combinations of coarse and fine screens and honeycombs of varying lengths. Two effects on the stream were detailed: honeycomb reduced the level of existing turbulence and at the same time generated turbulence of its own. Their initial tests indicated that the addition of a long, single honeycomb produced only a slight improvement in flow uniformity compared to an empty pipe, however both (long and short) honeycombs were effective in reducing pipe swirl.

Farrell et al's discussion suggests that in using a short honeycomb to reduce large-scale swirl motion and turbulence levels, it is beneficial to add a coarse screen upstream from the honeycomb so that the flow reaching the honeycomb cells is as uniform as possible. In addition to the coarse screen and honeycomb cell, a fine screen was added downstream to the combination. Results suggest that this combination further improves flow uniformity. Farell et al. also state that questions still remain on optimum honeycomb length and screen sizes.

Scheiman and Brooks [3] conducted an experimental test on a ½ scale model of an 8-foot pressure tunnel to examine turbulence reduction and compare results to theoretical analysis. They used various combinations of honeycomb and mesh screens as flow manipulators and located them in a square duct just after a bend. The turbulence reduction factor, f, was obtained by dividing the turbulence with manipulators installed by the turbulence without manipulators installed. Research indicated that the screens reduce axial turbulence more than lateral turbulence and that finer mesh screens gave a greater reduction in turbulence, while honeycomb alone or in combination with screens reduced lateral turbulence more than axial turbulence.

By comparing their results to theoretical data, their results compare well with those obtained by Prandtl's equation to determine the axial turbulence reduction factor,

$$f1 := \frac{1}{1 + K}$$

where K is the pressure loss coefficient and for lateral turbulence obtained by Dryden and Schubauer's relation,

$$f2 := \frac{1}{\sqrt{1 + K}}$$

Their data also indicates that screens downstream of a honeycomb cell have a better performance improvement than screens alone. Since turbulence downstream of a honeycomb cell is higher in the axial direction than the lateral direction and it is axial turbulence that screens are most capable of reducing, by locating the screen downstream of a honeycomb disturbances are further reduced.

As mentioned, honeycombs are flow conditioners that suppress the level of upstream turbulence. The suppression is mostly a reduction in the lateral components of the fluctuating velocity by the honeycomb sidewalls and is achieved a short distance downstream from the honeycomb entrance. New turbulence arises from the shear layer instability that occurs downstream of the honeycomb exit and increases with increasing honeycomb length. As a result, honeycombs of shorter length may be more beneficial. Also, honeycombs of shorter length experience less pressure loss.

An experiment was undertaken by Elder [15] to evaluate the effectiveness of porous-cell honeycombs to reduce turbulence in flow. The results of the porous-cell honeycomb were compared with results obtained from a solid cell honeycomb. The porous-cell honeycomb concept was developed by Vakili [5] to help improve honeycomb performance and to eliminate the honeycomb screen combination thereby reducing pressure losses. Each cell wall has holes that create flow passages between cells; this allows for the averaging of the total pressure differential between adjacent cells. The averaged total pressure differential between adjacent cells reduces the lateral and axial disturbances in the porous-cell honeycomb [15]. The porous section was located near the honeycomb entrance so as to reduce the additional disturbances that may be created by the flow passage between cells. Elder's results indicate that porous-cell honeycomb may be more effective than regular honeycomb at reducing turbulence.

Based on this finding, by applying the porous-cell honeycomb theory to curved ducts, the secondary flow caused by the curvature of the centerline may be significantly modified or reduced. As well, the duct length normally required to establish uniform flow after an elbow could be greatly reduced.

Dimensional Analysis

Dimensional analysis is used to help the experimentalist reduce the number of separate variables involved in a problem to a smaller number of independent dimensionless groups of variables. The variables important to this experimental study are:

D_p Diameter of Duct

L_p Total Length of Duct

R Radius of Curvature of Elbow

ε Surface Roughness of Duct

θ_1 Angle of 1st Elbow

θ_2 Angle of 2nd Elbow

l_{hc} Length of Honeycomb Cell

l_{pa} Length of Honeycomb Cell From Leading Edge to End of Porous Area

t	Honeycomb Cell Height
A_p	Porous Area of Honeycomb
A_T	Total Area of Honeycomb
ρ	Density of Fluid
μ	Viscosity of Fluid
U_∞	Free-Stream Velocity of Fluid
$\bar{U}$	MeanVelocity of Fluid
P_s	Local Static Pressure on Duct Wall
P_{ref}	Pressure at Inlet of Duct

The geometric characteristics of the duct with bends, the honeycomb and the mean velocity in the exit section of the duct are expressed in the following functional relationship:

$$F = f(D_p, L_p, R, \varepsilon, \theta_1, \theta_2, l_{hc}, l_{pa}, t, A_p, A_t, \rho, \mu, U_\infty, \bar{U}, P_s, P_{ref})$$

This system of 17 variables is reduced to 14 by using the Buckingham Pi Theorem [18] and the primary dimensions of mass, length, and time. The dimensionless pi, Π, groups are:

$$\Pi_1 = f(\Pi_2, \Pi_3, \Pi_4, \Pi_5, \ldots)$$

$$\Pi_1 = f(\theta_1, \theta_2, \varepsilon/D_p, L_p/D_p, R/D_p, \Delta P/\rho U_\infty^2, \mu/\rho\bar{U}l_{hc}, \mu D_p/\rho U_\infty R, \Delta P D_p/\rho U_\infty^2 L_p, \bar{U}/U_\infty, t/l_{hc}, l_{pa}/l_{hc}, A_p/l_{hc}^2, A_t/l_{hc}^2)$$

The amount of porous area, A_p, in the honeycombs was the only geometric variable in this experiment that varied from one configuration to the next. Four configurations of the honeycomb were tested and the amount of porosity in the cells ranged from 0% of the total area of the honeycomb cells to 40% of the total area of the honeycomb cells. In each configuration, the static pressure, P_s, and the mean velocity, $\bar{U}$ were measured in the exit section of the duct. Thus, the dimensionless variables that are pertinent to this experiment as a result of the geometric variables that change in the duct are:

$$\Pi_1 = f(\Pi_2, \Pi_3, \Pi_4, \Pi_5, \ldots)$$

$$\Pi_1 = f(\Delta P/\rho U_\infty^{\ 2}, \mu/\rho \bar{U} l_{hc}, \bar{U}/U_\infty, A_p/l_{hc}^{\ 2}, l_{pa}/l_{hc})$$

Chapter 3

Experimental Approach

3.1 Experimental Objectives

The objective of this study was to evaluate the effects of solid and porous-cell honeycomb to improve flow quality in curved ducts by reducing secondary flows. The experimental study consisted of 3 types of tests: pressure measurements, surface oil flow visualization, and Particle Imaging Velocimetry (PIV). Pressure transducers were used to measure the static pressure on the wall of the duct throughout the duct setup, surface oil flow visualization was used to obtain qualitative results to help justify the pressure measurement results, and PIV was used to determine flow characteristics such as the flow field velocity at the exit section after the 2nd elbow.

Solid honeycomb and porous-cell honeycombs were evaluated for their effectiveness in improving flow after the elbows and making the exit flow as uniform as possible. Elder [15] details the design and process of manufacturing the porous honeycombs. For each of the 3 types of tests, a baseline test-no honeycomb installed- was conducted to use as a basis of comparison to the tests involving the solid and porous-cell honeycombs. This comparison helped determine the effectiveness of using honeycomb as a flow control device. Results obtained from the porous-cell honeycomb were also analyzed to determine if the percentage of porosity was effective in improving the exit flow.

3.2 Experimental Setup

All experiments were conducted at the UTSI Aerodynamics and Propulsion Research Lab. A relatively simple apparatus was constructed to conduct the experiments. A pressure apparatus, which supplied the airflow, was connected to a 4-foot straight PVC duct by a concentric reducer. This 4-foot straight inlet section helped to ensure that the flow was fully developed prior to entering the first PVC 90° duct elbow. An upstream pipe length of 10D is normally sufficient to ensure fully developed uniform flow [4], however based on flow quality this is not always the case [4]; so, to achieve the greatest flow uniformity, a 12D pipe upstream of the 1st elbow was selected. The 4-foot straight duct connected to a PVC 90° duct elbow followed by a 6-inch section of straight PVC duct. The straight 6-inch duct connected to another PVC 90° duct elbow and led to a 4-foot straight PVC duct, which exited to the atmosphere. The 2 elbows created an offset in the flow. The duct geometry was selected because many industrial applications have numerous offsets in the flow and it was desired to imitate these designs as much as possible; as well, the offset created significant flow distortions making it the most extreme case of flow non-uniformity, any improvement in flow quality achieved in this configuration would be beneficial to any other geometry. Figure 1-1 (Chapter 1-p.3) illustrates the general setup of the duct. The duct had a constant inside diameter of 4-inches. A 4-inch diameter for the duct and elbow was selected because both items were commercially available and thus more cost-effective. The flanges that connected the straight ducts and elbows together were also commercially available in 4-inch diameter. Space limitations were considered in the design. A larger diameter throughout the duct would have been more expensive and would have occupied more space, without any major additional benefits.

Pressure measurements were conducted at speeds of 60ft/s, 80ft/s, and 100ft/s, while the surface oil flow visualization and the PIV tests were conducted at 100ft/s. Based on these speeds, the Reynolds number range was 127 204 – 212 007.

3.3 Instrumentation and Data Acquisition

3.3.1 Pressure Measurement System

The pressure transducers were used to measure the static pressure along the wall in the flow. Rosemount 1151DP pressure transducers were used. The pressure transducers were used to quantitatively measure the static pressure, with and without the honeycomb, at various locations along the duct. A comparison of results was undertaken to determine the effectiveness of the honeycomb, as well as comparing the effectiveness of the porosity of the honeycomb at improving the exit flow after the elbows.

A stainless steel tube, $1/16^{th}$ -in diameter and approximately 1-inch in length was tapped into the duct and connected to the Rosemount pressure transducer by a $1/16^{th}$ –inch diameter hose. Isolating diaphragms and oil fluid transmits pressure to a sensing diaphragm [19]. The sensing diaphragm is a stretched spring element, when the spring element deflects it responds to a pressure change. The displacement of the sensing diaphragm is proportional to the differential pressure [19]. At the same time, capacitor plates detect the position of the sensing diaphragm, which corresponds to an electrical signal. The signal is a change in voltage. LABVIEW software converts this voltage change to a recognizable static pressure.

Pressure ports were located longitudinally along the duct for 3 azimuth angles of 0°, 180°, and 270°. Figure 3-1 illustrates the orientation of the duct. The 0° azimuth angle corresponded to the outside wall of the 1^{st} elbow and the inside wall of the 2^{nd} elbow; the 180° azimuth angle corresponded to the inside wall of the 1^{st} elbow and the outside wall of the 2^{nd} elbow. Since separated flow originates on the inside wall of the elbow and the existence of secondary flow occurs closer to the outside wall, measurements were obtained along these azimuth angles to obtain quantitative data to explain the phenomena that occurred along these walls.

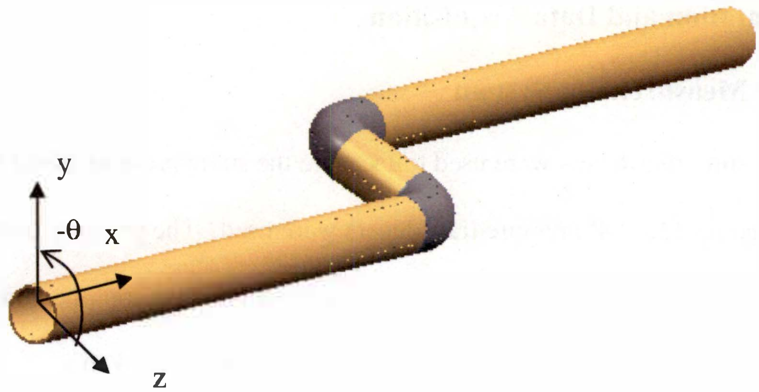

Figure 3-1. Duct Orientation

The inside bend however, formed a sharp 90° bend, thus the geometry was not conducive to obtain measurements along this wall. Ports were located immediately upstream and immediately downstream of this inside bend so that the flow pattern could be established. The 90° and 270° azimuth angles were symmetric along the x-z plane, therefore the same quantitative results would be obtained along either of these walls; as a result, measurements were obtained for only one angle (270°).

Figure 3-2 illustrates the pressure port locations along the duct wall. The first pressure port (not shown) was located at the inlet section of the first 4-foot duct, in close proximity to where the concentric reducer and the inlet duct connect. The first port at this location was consistently used as the free-stream reference pressure for all configurations and for the pressure coefficient, C_p, calculations.

Pressure measurements were located upstream of the 1st elbow in the inlet duct to determine if the flow experienced any upstream effect generated by the elbows. Ten pressure ports were located upstream of the 1st elbow, including the pressure port at the inlet of the duct (not shown) used as the free-stream reference pressure, discussed previously.

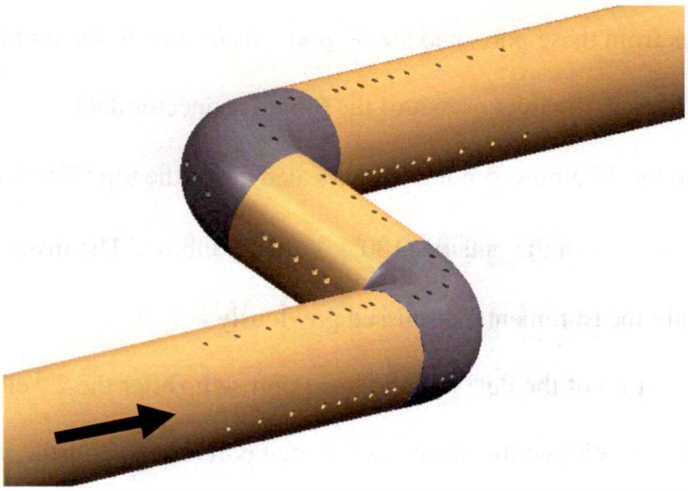

Figure 3-2. Pressure Port Locations Along the Duct

The next 4 ports were located 2-inches apart, starting 36-inches downstream of the inlet section. As the flow approached the elbow, the ports were located closer together to ensure that any significant changes in pressure were measured. From 42-inches to 46-inches downstream of the inlet section, 4 ports were located 1-inch apart. The last port ahead of the elbow was located 46.5-inches downstream of the inlet. It was desired to locate this port as close to the inlet of the elbow as possible but the flange that connected the straight duct to the elbow was 1.5-inches wide, thus it was not possible to obtain pressure measurements any closer to the inlet of the elbow. The flanges that connected the sections are not shown.

Five ports were located along the top of the 1st elbow (270°) and 7 ports were located on the outside of the 1st elbow (0°). No ports were located on the inside bend of the 1st elbow (180°) because the radius of curvature was short and the elbow too sharp, thus the geometry was not conducive to obtain measurements (as discussed previously).

Pressure measurements were obtained in 5 locations in the 6-inch connector duct joining the 2 elbows. Two ports were located each 1.5-inches from the ends; the width of the flange prevented any measurements from being obtained any closer to the ends. A port was located 0.5-inches from these ports and the 5th port was located in the middle of the duct at the 3-inch location from the inlet or exit of the 6-inch connector duct.

Similar to the 1st elbow, 5 ports were located along the top (270°) of the 2nd elbow and 7 ports were located on the outside (180°) of the 2nd elbow. The inside bend (0°) was not conducive to obtain measurements, discussed previously.

The exit section of the duct had the same port setup after the 2nd elbow, as the inlet section ahead of the 1st elbow; the distances between ports became further apart as distance downstream increased. Table B1-1 (Appendix B) details port locations in inches after inlet of the duct, as well the non-dimensional locations. Table B1-1 also details in which portion of the duct the port was located and for which azimuth angle.

The number of pressure transducers available for testing was limited, so the straight ducts were rotated every 90° to obtain measurements in the 0°, 180°, and 270° orientations.

Baseline: Pressure Measurement Configuration

There was no honeycomb installed in the duct for baseline measurements. Pressure measurements were taken at all locations throughout the setup discussed above. The initial test was conducted at 0° on the duct, after each test, the duct was rotated 90° to quantify the pressure at 180°, and 270°. Pressure measurements were also performed at the 0° and 270° positions along the 1st elbow and the 180° and 270° positions along the 2nd elbow.

Honeycomb After 1st Elbow: Pressure Measurement Configuration

A connector duct containing a 6-inch long honeycomb section replaced the 6-inch straight connector duct located between the 2 elbows. Tests were conducted with a solid honeycomb, a 20% porous-cell honeycomb, a 30% porous-cell honeycomb, and a 40% porous-cell honeycomb.

Pressure measurements were taken along the inlet duct wall at 270°, along the exit duct wall at 0°, 180°, and 270°, and along the 2nd elbow wall at 180° and 270°. Once these tests were completed, the 6-inch honeycomb section was replaced with the 6-inch empty connector duct.

Honeycomb After 2nd Elbow: Pressure Measurement Configuration

A 6-inch long honeycomb was added immediately after the 2nd elbow. Tests were conducted with a solid honeycomb, a 20% porous-cell honeycomb, a 30% porous-cell honeycomb, and a 40% porous-cell honeycomb.

Pressure measurements were taken along the exit duct wall at 0°, 180°, and 270° and along the 2nd elbow wall at 180° and 270°.

3.3.2 Flow Visualization

Surface oil flow visualization was conducted to achieve a better understanding of duct flow in this experimental configuration and to visualize what occurs as flow travels through the elbows. The surface oil flow visualization tests performed were qualitative and the results obtained from these tests were used to help justify the conclusions and quantitative results obtained with the pressure measurement tests.

In order to accurately record the results obtained in the surface oil flow visualization, a clear PVC pipe with the same inside diameter replaced the PVC pipe used to perform the pressure measurements. The clear PVC pipe enabled the flow visualization pattern to be photographed. The dye used for the surface oil flow visualization was a mixture of oil based paint and kerosene. The mixture needed to be viscous enough to remain on the duct walls but not too viscous that it would not follow the airflow. The mixture, once injected into the flow, followed the path that the flow traveled.

All flow visualization tests were performed at a speed of 100ft/s. Once the airflow was established at 100ft/s, the mixture was injected at every 20° around the duct using a needle. Once the last port was injected, the test continued for approximately one minute so that the flow pattern could be well established. After each test, digital photographs recorded the flow visualization pattern results; the duct was then taken apart and prepared for the next run.

Surface oil flow visualization was conducted for 5 configurations: baseline, solid honeycomb, 20% porous-cell honeycomb, 30% porous-cell honeycomb, and 40% porous-cell honeycomb. Although the baseline test analyzes flow throughout the duct, the main focus was on the exit section so as a comparison between baseline results and honeycomb results could be obtained. The non-baseline tests-tests with honeycomb-were conducted with the honeycomb sections installed immediately downstream of the 2nd elbow. This location was selected because it was assumed that a more uniform flow pattern would be achieved within a shorter distance downstream of the elbow. When the exit section of the flow with honeycomb installed was compared to the baseline, the same location downstream of the elbow was considered.

Baseline: Flow Visualization Configuration

One baseline test for flow visualization was conducted. Three locations along the setup contained injection ports: the inlet duct, the 6-inch straight connector duct, and the exit duct. The injecting ports on the inlet duct were located 2D upstream of the 1st elbow, every 20° around the pipe. The injection ports on the 6-inch straight connector duct were located 1.5-inches downstream of the beginning of the 6-inch pipe, every 20° around the duct. The injection ports on the exit duct were located 1.5-inches downstream of the 2nd elbow, every 20° around the duct.

Honeycomb After 2nd Elbow: Flow Visualization Configuration

The honeycomb sections were located after the 2nd elbow. The injection ports were located 1.5-inches downstream from the end of the honeycomb section, every 20° around the duct.

3.3.3 Particle Imaging Velocimetry (PIV) System

Particle Imagining Velocimetry (PIV) was used to measure the secondary flow field after the 2nd elbow. Similar to the tests involving pressure measurements and flow visualization, a comparison of results was undertaken to determine the effectiveness of the solid and porous honeycomb in eliminating the secondary flow and improving the exit flow after the elbows.

PIV is an optical technique used to measure the flow field velocity at certain planes in a flow. PIV uses two lasers that are pulsed at a specified time, forming a light sheet and illuminating the flow field, which is seeded with small smoke particles. A CCD camera records the smoke particle positions at each instant the lasers are pulsed.

The PIV system used by UTSI utilizes Twin Continuum ND: YAG lasers. The lasers have an output of approximately 200mJ at wavelengths of 532nm. The laser light beams are shaped by spherical and cylindrical optical lenses, when combined, produce a sheet of light that illuminates an area of the flow.

The CCD camera used is a TSI PIV CAM 10-30 with a 60mm FL F/2.8 Micro Nikkor Lens. The laser pulse synchronizer is the TSI 610032 synchronizer, which controls the laser and the camera.

A Pentium 3, PC computer with Windows NT 4.0 software and TSI Insight NT software is connected to the synchronizer. The Insight software contains selections for the user to control camera, laser, and data recording options.

Two Frame Cross Correlation technique is used to determine the smoke particle's velocity vector. The Cross-Correlation is two images, taken at specified times, (depending upon the spacing of the pulses) that can identify the movement of a particle from one image to the next image. By knowing the time interval between pulses, the image can be analyzed to determine the displacement of the particles and from these, the velocity of the particle.

The accuracy of the measurements depends on how well the seeds follow the flow. It is important in PIV that the seed particles are small enough to follow the flow's path but also it is important that the particles are large enough to generate scattered light when illuminated. Based on this criterion, the smoke particles were between 5-15μ and were injected far upstream in the pressure apparatus prior to the flow reaching the first duct. Figure 3-3 depicts the PIV setup.

PIV data was collected for 5 test configurations: baseline, solid honeycomb, 20% porous-cell honeycomb, 30% porous-cell honeycomb, and 40% porous-cell honeycomb. The PIV tests were performed 6-inches after the 2nd elbow in the duct. After the 2nd elbow, two 6-inch duct sections were installed. A gap of 1/8th -inch was left at the top between the 2 ducts so that the laser light sheet could illuminate the particles traveling through the duct. PIV measurements were taken immediately after the first 6-inch duct. For baseline measurements, the 6-inch duct after the 2nd elbow was empty. For the honeycomb PIV tests, the honeycomb replaced the 6-inch duct.

For each configuration, PIV captured 100 sets of data. Each data set consisted of 2 frames, the images taken 5μs apart. From the images, PIV software determined velocity vectors in the x-y plane. From this data, TecPlot was used to calculate the vorticity contours of each configuration. Since vorticity is the measure of rotation of a fluid, the contours were used to describe the fluid's motion; this gave a good indication of where the vorticity occurred in the duct.

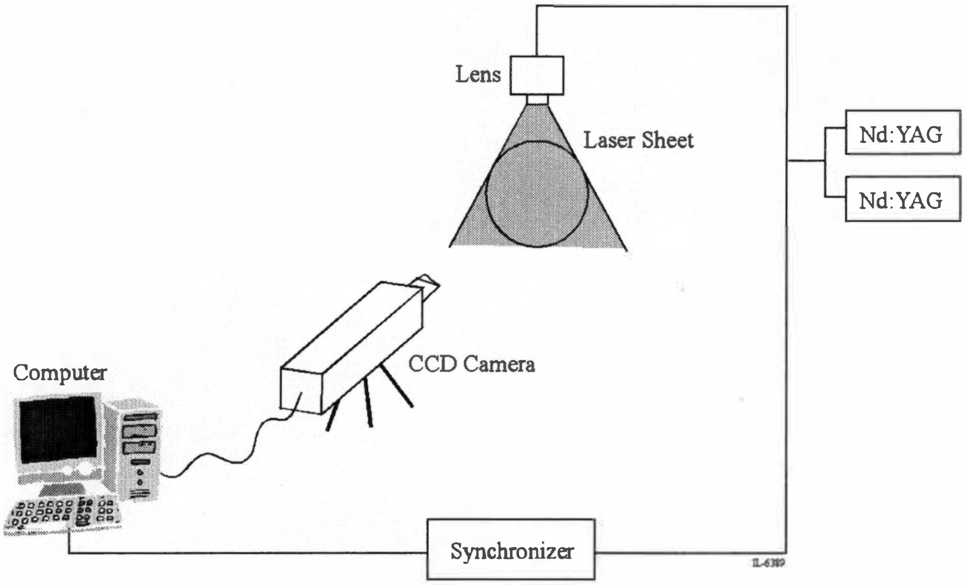

Figure 3-3. PIV Setup

Chapter 4

Results and Discussion

Numerous separate tests involving pressure measurements, flow visualization, and Particle Imaging Velocimetry (PIV) were conducted. Baseline measurements-no honeycomb installed- were performed for all measurement techniques. Once baseline tests were completed, tests were run with selected honeycomb installed at either of two locations, after the 1st elbow or after the 2nd elbow, within the duct; the focus being the effects of the honeycomb on the exit flow.

4.1 Flow Visualization

4.1.1 Baseline Flow Visualization

Two flow patterns, Figure 4-1, are revealed in the inlet section of the duct: uniform and swirl. The flow in the inlet section of the duct is uniform but as the flow approaches the 1st elbow, upstream effects begin to show. These upstream effects are due to the presence of the elbows and the secondary motion of the flow.

The flow pattern changes dramatically upon entering the 1st elbow, Figure 4-2. Very little dye mixture exists along the 180° wall of the duct as the flow moves into the elbow. The 180° elbow wall, which corresponds to the inside bend of the 1st elbow, is where flow separation originates and extends into the exit of the elbow. At 100ft/s free-stream velocity, this region of flow separation is large, as a result minimal dye mixture appears on the duct walls where flow separation occurs.

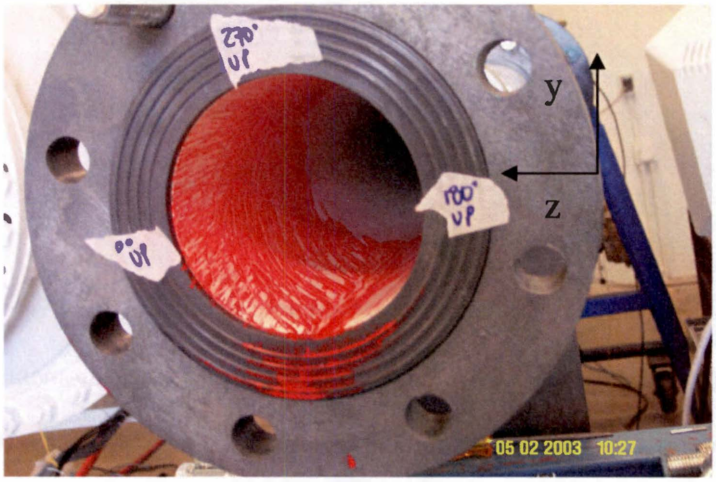

Figure 4-1. Inlet Pipe, Baseline

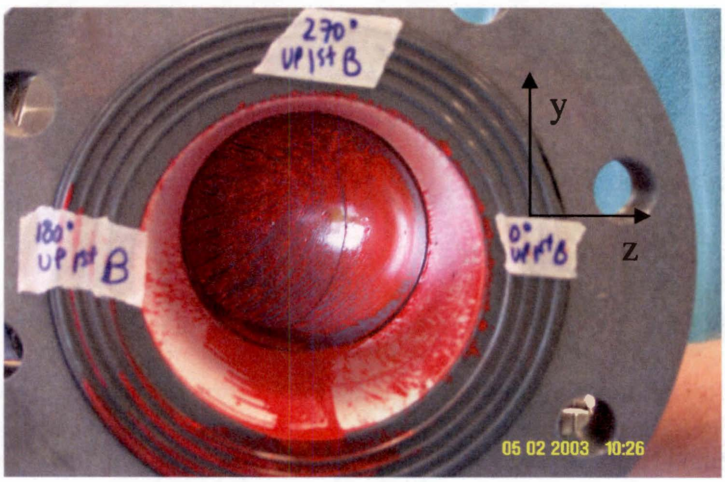

Figure 4-2. Upstream 1st Elbow, Baseline

The 0° elbow wall corresponds to the outside bend and is the area where secondary flow exists. The secondary flow causes the swirling motion of the flow and is expected to exhibit a strong swirling flow pattern on the duct walls. Figure 4-2 illustrates the onset of the swirling motion of the flow as it moves from the outside bend towards the exit of the duct elbow. The 100ft/s free-stream velocity tested is a high-energy flow. As the high-energy flow moves through the elbow, it forces the secondary flow towards the opposite duct wall. As a result, the low energy flow (separated flow) is pushed further into the exit of the elbow and into the 6-inch connector duct by the momentum of the oncoming flow; the result is a large region of flow separation.

As the flow moves further through the 6-inch connector duct, the strength of the swirl pattern diminishes slightly but still exists prior to entering the 2nd elbow. The decay in the swirl signifies that the flow has tried to reestablish uniformity, Figure 4-3, but the 6-inch connector duct is not long enough to reduce the significant disturbances and to establish a fully uniform flow.

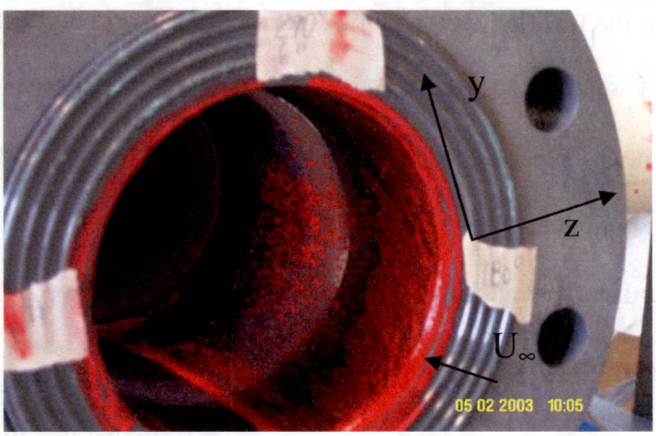

Figure 4-3. 6-Inch Connector Duct, Baseline

Prior to the flow reaching the end of the 6-inch connector duct, the already highly non-uniform flow also begins to experience upstream effects from the 2nd elbow. The upstream effects contribute to the swirl pattern of the flow entering the 2nd elbow, Figure 4-4. Because the duct is axisymmetric about the x-z plane, it was expected that the same flow pattern would be exhibited on the upper and lower halves of duct. Figure 4-4 illustrates that this is not the case; the secondary flow pattern is only on one half of the duct indicating that gravity played a significant role in the results obtained with surface oil flow visualization.

In the 2nd elbow, the same trend as when the flow entered the 1st elbow is exhibited, except the disturbances in the 2nd elbow are coupled with the non-uniformities of the 1st elbow. As the flow leaves the 2nd elbow and enters the exit section of the duct, the flow is highly non-uniform as a result of the axial and lateral disturbances generated by the elbows and forced further downstream by the oncoming high-energy flow.

Figure 4-5 illustrates the flow when it first enters the exit section of the duct. The flow is highly non-uniform possessing a strong secondary flow. The 180° and 0° duct walls of the exit section are shown in Figures 4-6 and 4-7. Both sides of the duct wall exhibit significant swirl as the flow leaves the elbow. As mentioned, gravity contributes to the flow pattern established. Only one half of the duct exhibits the flow pattern generated by secondary flows; it was expected that the upper and lower halves of the duct would have a symmetric pattern but due to gravity effects, this did not occur.

4.1.2 Flow Visualization with Honeycombs After 2nd Elbow

4.1.2.1 Solid Honeycomb Flow Visualization

Along the 180° wall of the exit duct, the dye mixture that was injected after the solid honeycomb exhibits two opposing flow patterns: 1. a straight flow, and 2. a counterclockwise swirl pattern, Figure 4-8.

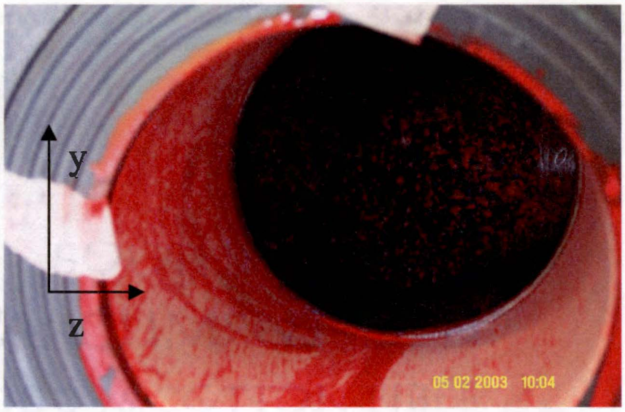

Figure 4-4. Upstream 2^{nd} Elbow, Baseline

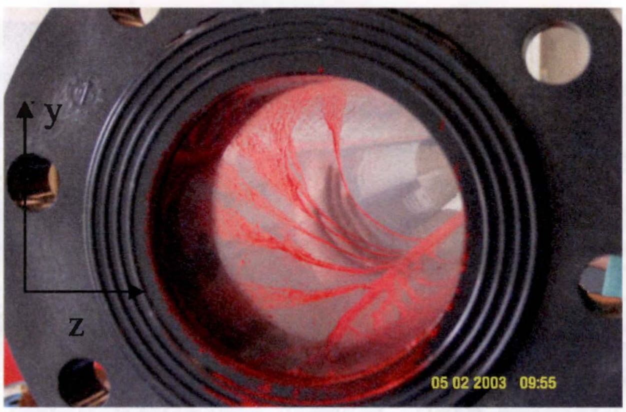

Figure 4-5. Exit Duct, Baseline

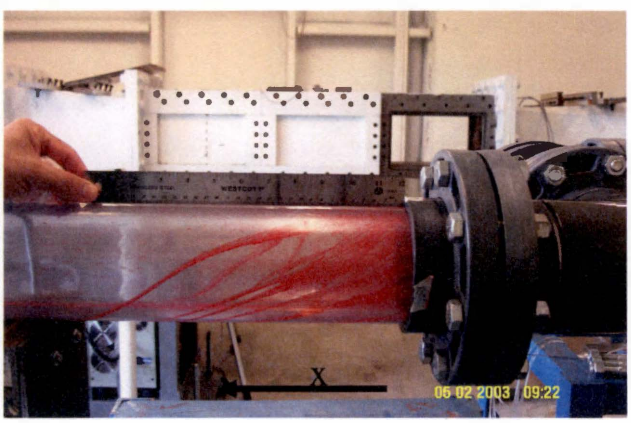

Figure 4-6. Exit Duct 180°, Baseline

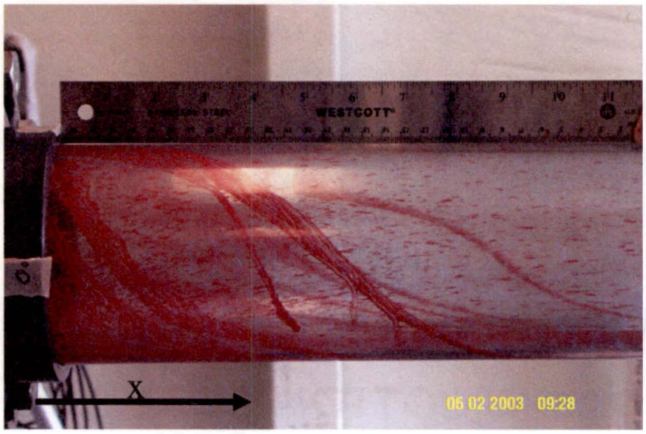

Figure 4-7. Exit Duct 0°, Baseline

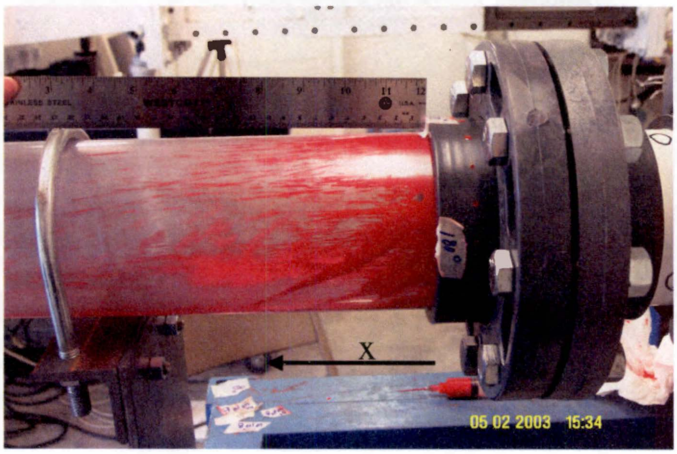

Figure 4-8. Exit Duct 180°, Aft Solid Honeycomb

The swirl pattern suggests that the flow leaving the honeycomb cell and entering the exit duct still contains non-uniformities that were generated by the elbows. The high-energy flow that moves through the 1st elbow forces the non-uniformities further into the elbow exit and into the 6-inch connector duct. The 6-inch connector duct is not long enough to reduce the significant disturbances and to establish uniform flow. Thus, the flow entering the 2nd elbow is a highly non-uniform flow. The 2nd elbow generates its own non-uniformities; as a result, the flow entering the solid honeycomb has coupled disturbances from the 1st and 2nd elbows.

The flow that passes through the honeycomb cells along the 180°-duct wall is the non-uniform flow from the 1st elbow forced to travel through the duct by the high kinetic energy flow, as well as the secondary flow generated on the outside bend of the 2nd elbow. Because the extent of non-uniformities was extreme, flow still contains some disturbances that were not eliminated by the solid honeycomb. This is the reason the 180° area of the duct wall contains a larger area of swirl. These results are compared to the exit section of the baseline flow, Figure 4-7, Sec 4.1.1. A more dominant swirl pattern as discussed in Sec 4.1.1 is evident. The flow after the solid honeycomb section exhibits more flow uniformity and less swirl than the baseline results, indicating that the solid honeycomb was successful in removing some of the non-uniformities in the flow generated by the elbows. Gravity effects contribute to the asymmetric flow pattern on the duct walls.

In the 0° orientation, along the wall of the duct, no distinguishable flow pattern exists, Figure 4-9, immediately after the exit of the honeycomb section. The separated flow that occurs in the 2nd elbow originates on the inside bend and extends into the exit section. The flow that passes through this section of the honeycomb is separated flow. This is the reason that no flow pattern is observed on the duct walls immediately after the solid honeycomb. Further downstream of the exit section of the duct, a flow pattern begins to develop.

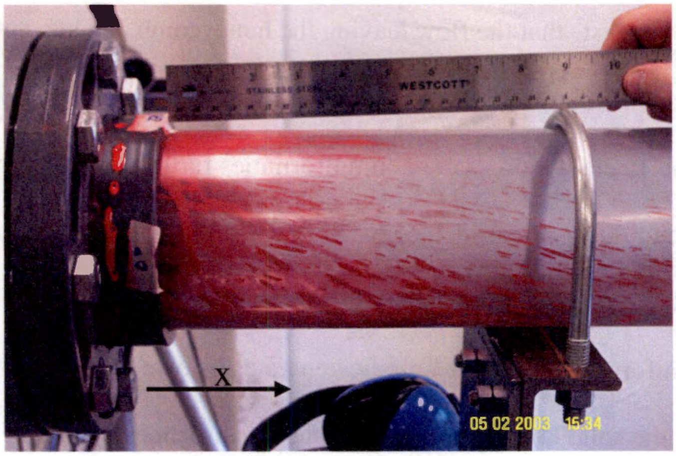

Figure 4-9. Exit Duct 0°, Aft Solid Honeycomb

There is slight evidence of the flow wanting to swirl, however the solid honeycomb prevents a strong swirling flow from forming by eliminating many of the disturbances in the flow. Compared to the baseline flow, Figure 4-7, there is more flow uniformity apparent when the solid honeycomb is installed. The baseline flow, at the same location downstream of the elbow, exhibits a larger swirl pattern; although the strength of the swirl has decayed significantly compared to when it first exited the elbow, the flow experiences more losses in the process as it tries to recover from the disturbances.

Along the duct wall at azimuth angle 270°, Figure 4-10 illustrates more completely the flow pattern that occurs in the exit section. This picture shows that the flow is more uniform entering the exit section of the duct and moving downstream. In the baseline flow however, as the flow moves downstream, the mixture swirls towards the outside of the duct and accumulates at the bottom (90°) of the duct due to gravity effects.

Comparing the flow in the 3 angles along the duct wall, the flow is near uniform in the 0° and 270° orientations while the 180° orientation exhibits more swirl pattern in the flow.

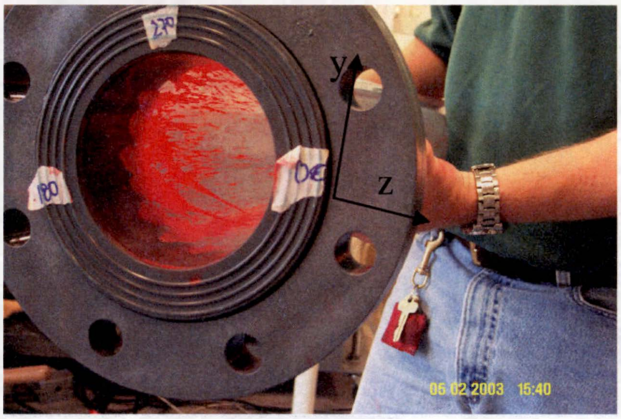

Figure 4-10. Exit Duct, Aft Solid Honeycomb

The solid honeycomb helped to eliminate the coupled non-uniformities generated by the elbows; however at the high free-stream velocity, the flow separation that occurred was extreme and as a result, the solid honeycomb was able to eliminate only some of the disturbances in the flow.

4.1.2.2 20% Porous-Cell Honeycomb Flow Visualization

The 20% porous-cell honeycomb located after the 2nd elbow exhibits very similar results to that obtained with the solid honeycomb.

Along the 180° duct wall, Figure 4-11, the two flow patterns discussed in Sec 4.1.2.1 are present. Similar to the solid honeycomb discussed in Sec 4.1.2.1, the 20% porous-cell honeycomb is unable to eliminate all the non-uniformities generated by the large areas of flow separation in the 1st and 2nd elbows at the high free-stream velocity. As the flow moves further downstream, the swirl decays and flow uniformity becomes more apparent. The reasons behind the large swirl pattern that is still present along this duct wall are discussed in Sec 4.1.2.1.

Along the 0° duct wall with the 20% porous-cell honeycomb installed, Figure 4-12, exhibits the same results as those obtained with the solid honeycomb.

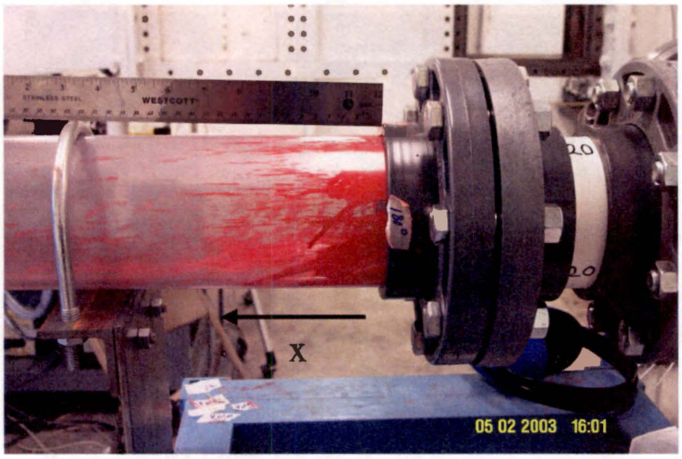

Figure 4-11. Exit Duct 180°, Aft 20% Porous-Cell Honeycomb

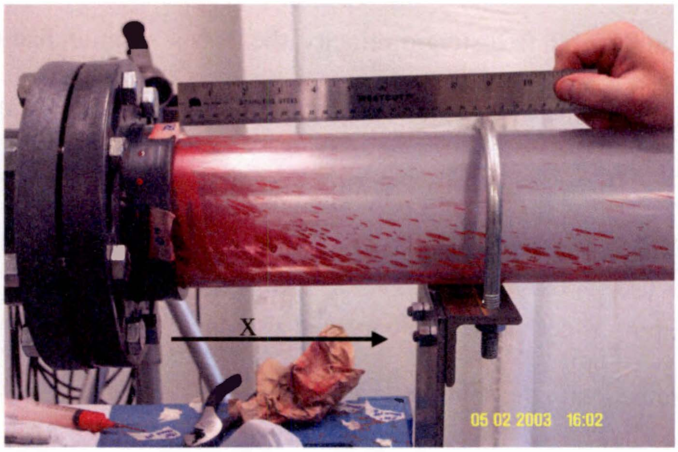

Figure 4-12. Exit Duct 0°, Aft 20% Porous-Cell Honeycomb

Although the dye mixture was thick and the flow pattern was not as distinguishable as desired, it was still apparent that the flow did not have a large swirl pattern because, as discussed in Sec 4.1.2.1, the flow passing through this section of the honeycomb was separated flow. As the flow moves further downstream, the flow becomes more uniform.

Along the 270° duct wall, flow has a tendency to begin to swirl, however the dye mixture was too thick for the flow to follow its desired path. At the same time, uniform flow is also present in the flow as shown in Figure 4-13. From the theory of porous-cells, the porous-cells reduce axial and lateral disturbances in the flow by averaging the total pressure differential between adjacent cells. The non-porous cells help to further reduce the lateral disturbances in the flow. As the flow moves downstream, uniformity is more dominant than at the same location in the baseline flow.

As discussed in Sec 4.1.2.1, the honeycomb helps to eliminate some of the flow non-uniformities generated by the elbows. At the high free-stream velocity however, the extent of flow separation and secondary flow is extreme resulting in the 20% porous-cell honeycomb being unable to obtain a completely uniform flow, however within a short distance downstream flow uniformity is achieved. Once again, the asymmetric flow pattern on the duct wall was a result of gravity effects.

Figure 4-13. Exit Duct 270°, Aft 20% Porous-Cell Honeycomb

4.1.2.3 30% Porous-Cell Honeycomb Flow Visualization

Figure 4-14 illustrates the swirl pattern more significantly than the solid honeycomb and 20% porous-cell honeycomb along the 180° duct wall. Since the dye mixture was less viscous, it was able to follow the flow's path more easily; however gravity effects still contributed to the asymmetric flow pattern on the duct walls. This flow pattern is very similar to the baseline; however with the 30% porous-cell honeycomb the swirl is not as dominant and the flow becomes uniform much more quickly than the baseline. A slightly larger swirl pattern than the solid honeycomb is exhibited, possibly due to the upstream history of the flow. The more porous honeycomb may generate more significant upstream effects in the elbow than the less porous or non-porous honeycomb. As a result, the flow may experience more losses as it travels through the elbow and the honeycomb section. Although the flow exhibits slightly more swirl, the disturbances subside quickly and the flow becomes more uniform within a shorter distance downstream.

In the 0° orientation, the same flow pattern as exhibited with the solid honeycomb and 20% porous-cell honeycomb is present, Figure 4-15. The flow contains a very small amount of swirl and becomes uniform within a short distance downstream of the honeycomb section, Sec 4.1.2.1.

Figure 4-14. Exit Duct 180°, Aft 30% Porous-Cell Honeycomb

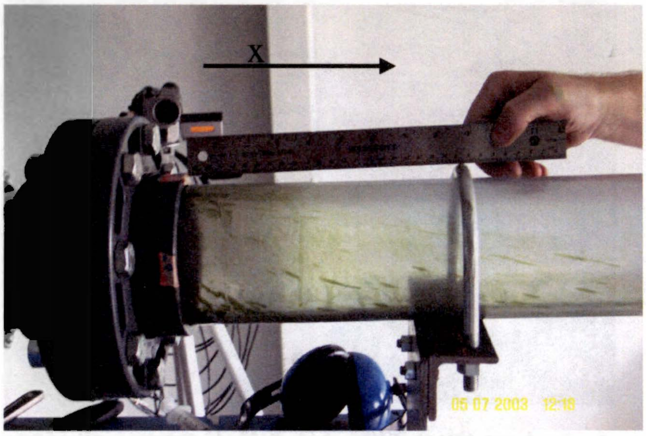

Figure 4-15. Exit Duct 0°, Aft 30% Porous-Cell Honeycomb

The 270° duct wall helps to illustrate the rapid decay in the swirl pattern of the flow as it leaves the honeycomb section, Figure 4-16. Compared to the baseline flow, there is a significant improvement in flow uniformity at the same location downstream of the elbow. In other words, uniform flow is achieved within a shorter distance downstream of the elbow when the 30% porous-cell honeycomb is installed.

Overall, the 30% porous-cell honeycomb demonstrated the flow pattern leaving the honeycomb more successfully than the solid or 20% porous-cell honeycomb. The dye mixture used was more conducive to following the flow's path. Surface oil flow visualization illustrated that the 30% porous-cell honeycomb was able to eliminate some of the non-uniformities generated by the 2nd elbow and create a uniform flow within a shorter distance downstream of the elbow. As discussed in Sec 4.1.2.1, the high free-stream velocity generates a very large area of flow separation in the elbow; because of this, the flow is highly non-uniform. Although the 30% porous-cell honeycomb is able to remove some of these non-uniformities compared to those of baseline, the still present swirl pattern signifies that non-uniformities still exist until further downstream of the honeycomb exit.

Figure 4-16. Exit Duct 270°, Aft 30% Porous-Cell Honeycomb

4.1.2.4 40% Porous-Cell Honeycomb Flow Visualization

Surface oil flow visualization with the 40% porous-cell honeycomb illustrates most clearly, flow behavior as it leaves the honeycomb section and enters the exit duct.

The most dominant flow pattern exists along the 180° duct wall, Figure 4-17. A distinguishable counterclockwise swirl pattern exists. Although the swirl pattern appears large, the disturbances are very weak; as a result, the swirl dissipates quickly, and a more uniform flow is established within a shorter distance downstream. Sec 4.1.2.3 discusses the possibilities for the larger swirl pattern with the more porous-cell honeycomb installed.

Similar to the 30% porous-cell honeycomb, Sec 4.1.2.3, along the 0° duct wall little swirl is present and significant flow uniformity exists, Figure 4-18.

All the honeycombs were successful in removing the non-uniformities in the flow generated by the elbows, however the 40% porous-cell honeycomb helped to generate a more uniform flow, eliminating more of the flow non-uniformities. Because the extent of flow separation was extreme at the high velocity, the honeycombs were only able to remove some of the disturbances in the flow. By removing some of the non-uniformities, a higher local velocity occurs in the exit section of the duct. As well, the honeycomb helped to establish a uniform flow in a shorter distance downstream than the baseline flow.

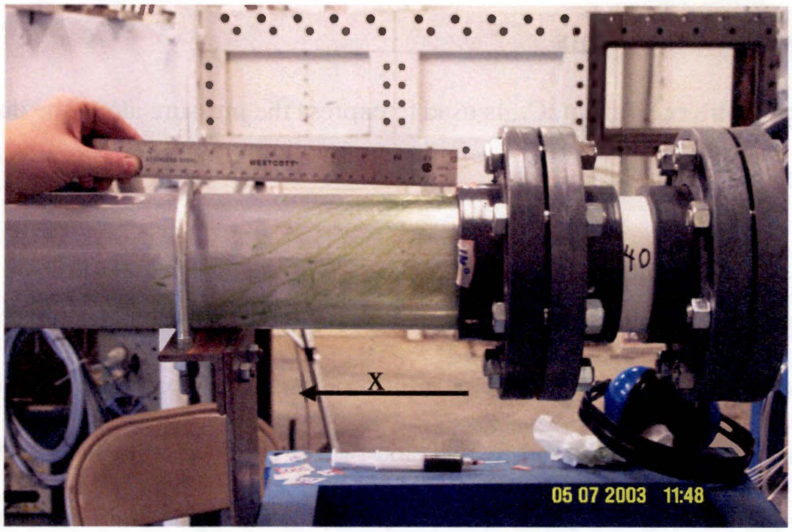

Figure 4-17. Exit Duct 180°, Aft 40% Porous-Cell Honeycomb

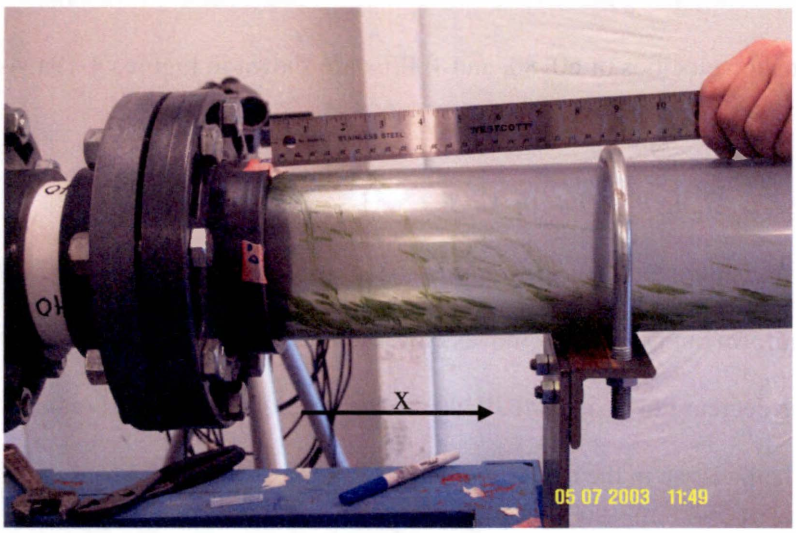

Figure 4-18. Exit Duct 0°, Aft 40% Porous-Cell Honeycomb

4.2 Pressure Measurements

The pressure coefficient, C_p, is used to express the pressure along the duct wall in non-dimensional form. It is defined as:

$$C_p = (P_s - P_{ref}) / (1/2)\rho U_\infty^2$$

By determining the non-dimensional pressure distribution, $C_{p,}$ at each point and plotting the value against its respective port location, L/D, flow patterns are determined. The port locations are non-dimensional, with L the measured distance in inches after the origin (the origin being the inlet of the first 4-foot duct), and D the inside diameter of the duct.

4.2.1 Baseline Pressure Results

Non-dimensional pressure distributions, for the baseline configuration (no honeycomb present), along the duct for three azimuth angles of 0°, 180°, and 270° and for three free-stream velocities of 60, 80, and 100ft/s are shown in Figures 4-19a, 4-19b, and 4-19c.

Pressure Results Along 0° Azimuth Angle

The measurements indicate, Figure 4-19a, that the flow through the inlet section of the duct is uniform but as the flow moves closer to the 1st elbow, the C_p begins to decrease slightly. This decrease in C_p is partially due to the development of the boundary layer resulting in the increase in the centerline velocity and also due to an upstream effect of the elbows as the flow approaches the 1st elbow. Flow pattern, as observed from surface oil flow visualizations, in the inlet section of the duct, is shown in Figure 4-1. In the inlet section, flow is basically straight with a small amount of swirl as the flow approaches the 1st elbow.

As the flow moves into the 1st elbow, a precarious variation in C_p exists for the 3 free-stream velocities tested.

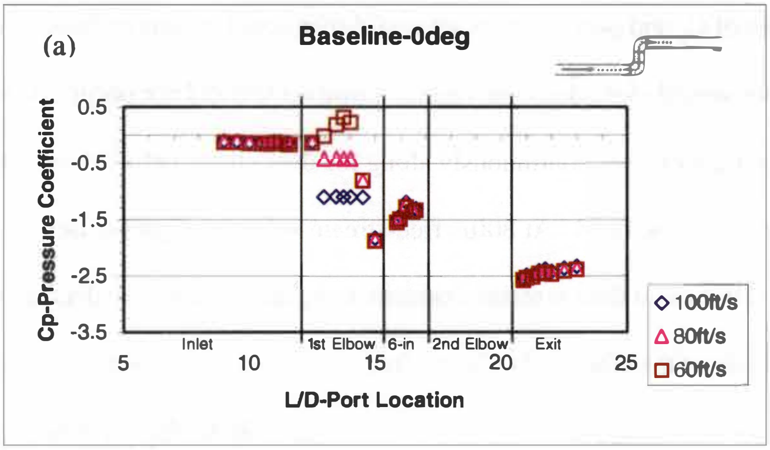

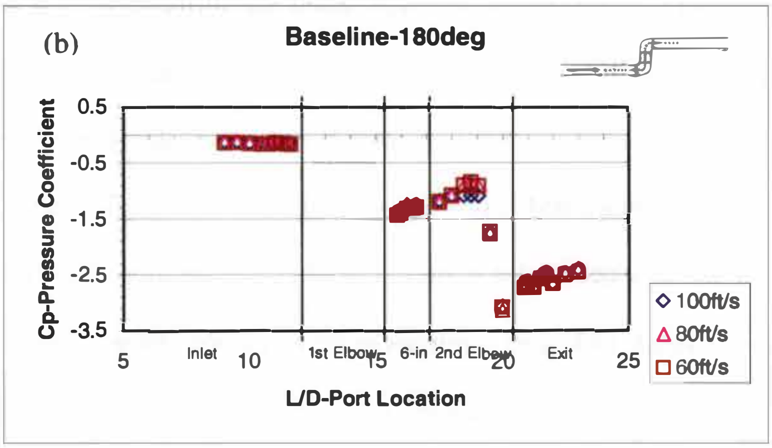

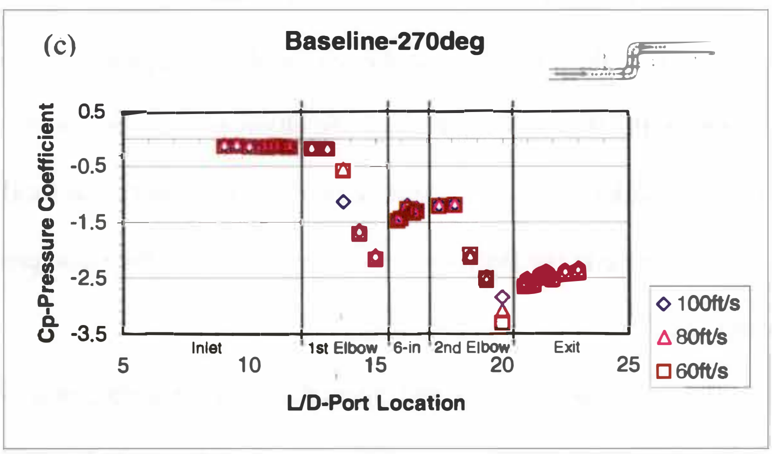

Figure 4-19. C_p vs. L/D-Baseline

Since the values of C_p and port location are non-dimensional, it was expected that the 3 free-stream velocities would yield the same results, however this did not occur. At 60ft/s free-stream velocity, C_p increases continuously along the duct elbow before decreasing just beyond the outside of the bend. At 80ft/s free-stream velocity, C_p decreases suddenly at the entrance of the elbow and then remains constant along the bend before decreasing, again just beyond the outside of the elbow. At 100ft/s free-stream velocity, a similar trend to that obtained at 80ft/s occurs, however as the flow enters the elbow, the decrease in C_p as well as the region of constant C_p is larger than that experienced by the flow at 80ft/s. The trend differences, between the 3 free-stream velocities tested, are attributed to flow separation on the inside of the bend and the existence of secondary flow that occurs because of the imbalance of centripetal forces as a result of the curvature of the duct centerline.

The constant C_p illustrated in this region (Figure 4-19a) signifies that no acceleration or deceleration of the flow occurs due to the extent of flow separation. The flow separation begins on the inside bend (180°) and continues to the exit of the elbow. The results indicate, Figure 4-19a, that as the free-stream velocity increases, the area of flow separation becomes larger and encompasses more of the duct. The decrease in C_p as the flow reaches the region of flow separation is due to the conservation of mass or continuity. The flow that enters the elbow must also leave the elbow but because the region of flow separation encompasses a certain area of the duct, the flow moving through the elbow past the region of flow separation must do so through a smaller area. As a result, to maintain continuity, the local flow velocity must increase. The increase in the flow's local velocity decreases the static pressure and results in a lower C_p.

Once the flow exits the 1st elbow and enters the 6-inch straight connector duct, it tries to recover from the effects of the elbow: -flow separation, -and the swirling secondary flow. The flow diffuses and fills the 6-inch duct. This results in a decrease in the local velocity of the flow and an increase in C_p. As the flow moves through the 6-inch duct, the recovery continues from the non-uniformities in the flow generated by the elbow. The variations in C_p however, indicate that the 6-inch duct is not long enough to establish uniform flow. Upstream effects of the 2nd elbow also begin to impact the flow as indicated by the slight decrease in C_p as the flow approaches the 2nd elbow.

No pressure measurements were obtained along the 0° azimuth angle of the 2nd elbow. As discussed in Sec 3.3.1, the radius of curvature of the inside bend is short, with a sharp 90° bend, thus the geometry of the inside bend was not conducive to obtain pressure measurements. The 0° wall of the 2nd elbow corresponds to the 180° wall of the 1st elbow. This is the region where flow separation begins and extends into the inside of this bend. It is expected that a similar trend to that exhibited in the 1st elbow will occur, however the region of flow separation may be even more extensive because of the oncoming highly non-uniform flow.

In the exit section of the duct, there is recovery of the flow from the effects of the upstream elbows. Because flow separation cannot continue long past the exit of the 2nd elbow area, the flow diffuses and thus fills the entire straight exit duct. This is illustrated by the increase in C_p as the flow enters the exit section. The flow is trying to recover from the non-uniformities generated by the 2nd elbow. As a result, variations in C_p exist. As the flow moves further downstream, the variations in C_p become less as the non-uniformities and swirl in the flow diminish. In the baseline flow, 0° along the duct, the flow has not become uniform by the end of the measurement region, however the trend indicates that the non-uniformities have diminished.

Pressure Results Along 180 °Azimuth Angle

The same results as discussed along the inlet of the 0° duct wall are obtained along the 180° wall, Figure 4-19b. In the inlet section of the duct, refer to 0° azimuth angle.

No measurements were obtained along the 180° wall of the 1st elbow, as a result of the geometry of the inside bend, Sec 3.3.1.

As the flow moves from the 1st elbow into the 6-inch straight connector duct, it tries to recover from the region of flow separation encountered in the 1st elbow. As detailed previously, the region of flow separation encompasses a portion of the duct elbow forcing the flow to move through a smaller area. From continuity, the local flow velocity must increase moving past this region since the same flow entering the elbow must leave the elbow. In the 6-inch connector duct, the flow then diffuses to fill the duct and the local flow velocity decreases, resulting in an increase in C_p. This is the same trend as exhibited along the 0° wall of the 6-inch duct, however the decrease in C_p is more gradual along the 180° wall as the flow moves through the duct. This could be a result of the extent of the flow separation and existence of secondary flow and how far it extends into the exit section of the elbow. The further these regions extend into the exit of the elbow, the greater the non-uniformities in the flow.

As the flow moves into the 2nd elbow, the flow patterns differ between the free-stream velocities tested, Figure 4-19b. The 100ft/s free-stream velocity illustrates a constant C_p along the wall of the elbow before decreasing and exiting the elbow; whereas, the lower free-stream velocities exhibit a continuous increase in C_p along the elbow wall before decreasing just beyond the outside of the elbow. Similar to the previous discussions along the 0° wall of the 1st elbow, (which corresponds to the outside wall of the 1st bend), the different trend in C_p between the free-stream velocities tested is attributed to the extent of the region of flow separation in the elbow. At 100ft/s free-stream velocity, the constant C_p in this region indicates no acceleration or deceleration in the flow due to the extent of flow separation. The significant decrease in C_p, at all the free-stream velocities tested, as the flow exits the elbow, is a result of continuity as previously discussed.

As the flow moves through the exit section, the local flow velocity decreases as the flow diffuses to fill the duct. In the straight exit section, the flow tries to recover from the non-uniformities generated by the elbow. By the end of the region of pressure measurements, the flow still has not become uniform but fewer losses occur as illustrated by only slight variations in C_p.

Pressure Results Along 270°Azimuth Angle

The trends, Figure 4-19c, exhibited along the 270° wall of the straight ducts are similar to the trends along the 0° wall of the straight ducts. The differences exist in the measurements and trends obtained along the elbows.

As the flow moves along the 270° wall of the 1st elbow, Figure 4-19c, C_p decreases. All the free-stream velocities tested have the same C_p values as the flow moves through the elbow with the exception of one point in the elbow where the 100ft/s free-stream velocity differs, Figure 4-19c; this illustrates that at the high free-stream velocity, flow separation affects the flow throughout the elbow.

Along the 2nd elbow, the trend is very similar, however the region of flow separation affects all the free-stream velocities tested as the flow exits the elbow. The flow that originates on the inside bend expands to fill more of the duct and extends into the exit section of the elbow. Since the flow entering the 2nd elbow is highly non-uniform as a result of the 1st elbow, the region of flow separation moves further into the exit section at all free-stream velocities tested.

Baseline tests reveal that the flow is significantly affected by the elbows, in particular the region of flow separation and the existence of secondary flow in the elbows. The difference in C_p values obtained along the elbows between the free-stream velocities tested is attributed to the extent of flow separation that occurs in the elbow. Of the free-stream velocities tested, the high free-stream velocity has a larger impact on the extent of the flow separation that occurs. Flow that has moved past the region of flow separation and into the straight ducts exhibits an increase in C_p as the flow diffuses filling the duct. This flow is also trying to recover from the non-uniformities generated by the elbows. The flow exhibits fewer variations in pressure but still has not become fully uniform by the end of the measurement region in the duct exit.

4.2.2 Pressure Results with Honeycombs After 1st Elbow

Four configurations were tested at 3 free-stream velocities. In each configuration static pressure measurements were obtained along the duct for 3 azimuth angles: 0°, 180°, and 270°. The main focus was on pressure measurements obtained in the exit section, however measurements were also obtained in the inlet section to determine if the honeycomb generated any upstream effects and in the 2nd elbow to determine the honeycomb's effect on flow entering the 2nd elbow.

4.2.2.1 Solid Honeycomb Pressure Results

Non-dimensional pressure distributions, for the solid honeycomb located after the 1st elbow, along the ducts 3 azimuth angles of 0°, 180°, and 270° and for the free-stream velocities of 60ft/s, 80ft/s, and 100ft/s are shown in Figures 4-20a, 4-20b, 4-20c, and 4-20d.

Pressure Results Along 0° Azimuth Angle

Figure 4-20a illustrates that for all the free-stream velocities tested, C_p is lower than the baseline values when the solid honeycomb is installed.

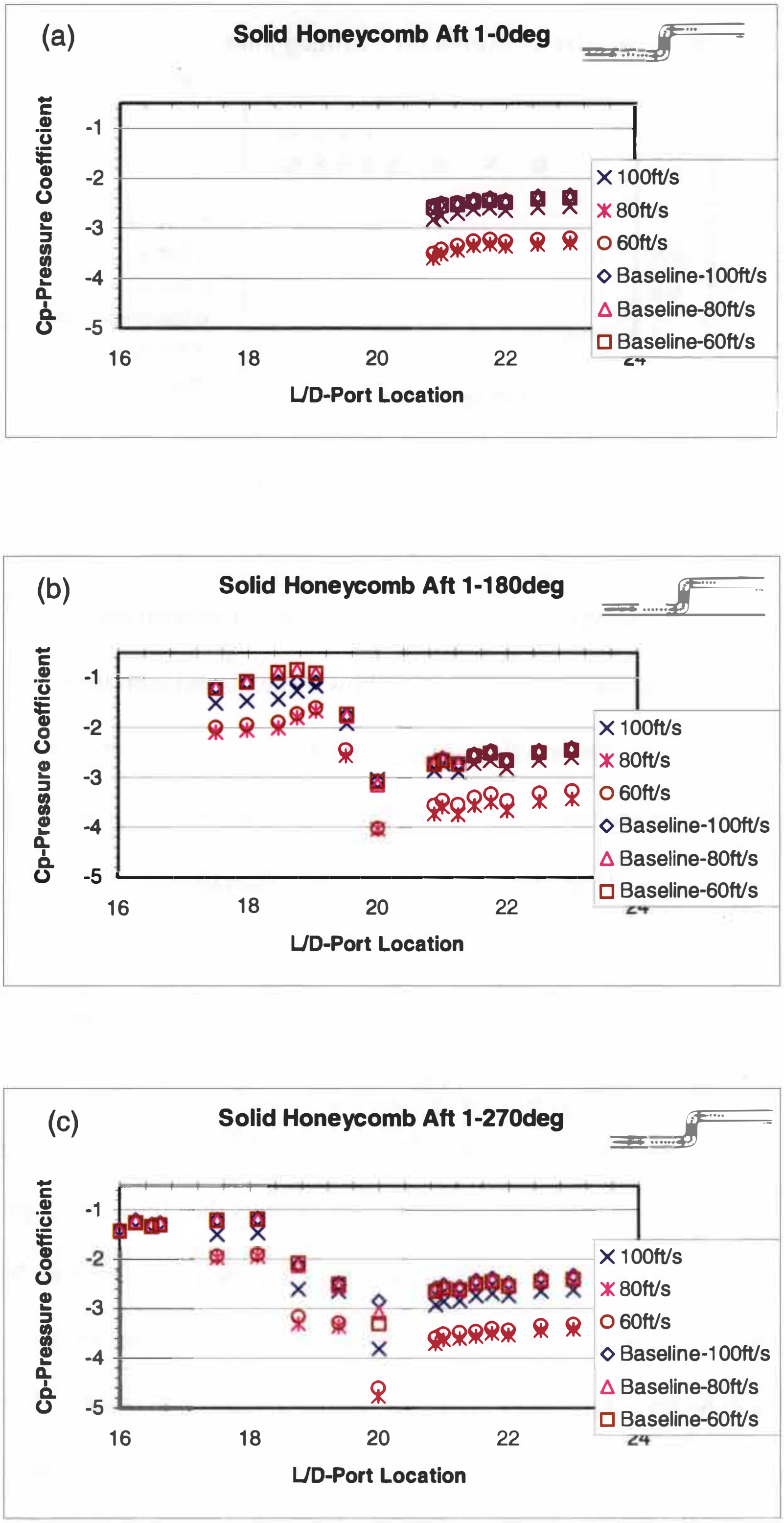

Figure 4-20. C_p vs. L/D-Solid Honeycomb Aft 1st Elbow

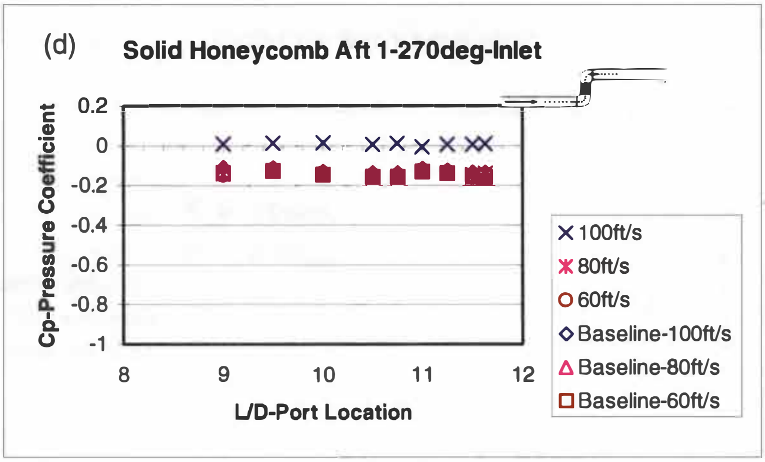

Figure 4-20. Cont'd

The flow that enters the solid honeycomb section is a highly non-uniform flow attributed to secondary flow and flow separation in the 1st elbow. The honeycomb helps to redistribute the flow and generate a more uniform flow with a higher local velocity entering the 2nd elbow. The more uniform flow entering the 2nd elbow also translates into a more uniform flow entering the exit section. Thus, the C_p values are lower than the baseline in the exit section of the duct.

Figure 4-20a also illustrates a difference in C_p values between the 3 free-stream velocities tested. From baseline results, it is known that the higher free-stream velocity experiences significant flow separation in the 1st elbow. The high free-stream velocity flow possesses a high kinetic energy. When the flow encounters the elbow, the high energy flow forces the non-uniformities that develop in the elbow into the exit section of the elbow and into the 6-inch connector duct. The higher the kinetic energy, the further the non-uniformities will be forced to travel. With the solid honeycomb located in the position of the 6-inch connector duct, it is able to improve the flow entering the 2nd elbow by redistributing the flow and eliminating some of the disturbances. However, at the high free-stream velocity it is not able to eliminate all the non-uniformities generated prior to entering the 2nd elbow since they are so extreme. As a result of the still present non-uniformities, the flow entering the 2nd elbow has a lower local velocity and a higher C_p than the flow at the lower free-stream velocities tested.

The non-uniformities that were not removed by the solid honeycomb enter the 2nd elbow and contribute to the flow separation and secondary flow that occurs. The region of flow separation that originates on the inside of the duct elbow extends into the exit of the elbow and possibly into the exit duct depending on the extent of flow separation.

The increase in C_p at the beginning of the exit section is a result of the flow diffusing to fill the exit duct as it recovers from the secondary flow and flow separation in the 2nd elbow. As well, the flow is trying to return to a uniform flow; as a result of the losses in trying to establish uniformity, variations in C_p exist. By the end of the pressure measurement region, the flow has not achieved uniformity but the variations in C_p have diminished indicating that slightly further downstream the flow will become uniform.

Pressure Results Along 180°Azimuth Angle

As the flow moves through the 2nd elbow, the C_p for all free-stream velocities tested is lower than the baseline values, Figure 4-20b. The solid honeycomb redistributes the non-uniformities in the flow generated by the 1st elbow prior to the flow entering the 2nd elbow, as previously discussed. As a result, the flow leaving the solid honeycomb is more uniform with a higher local velocity and lower static pressure as it travels into the 2nd elbow.

All 3 free-stream velocities tested exhibit the same trend as the flow moves through the elbow, however the 100ft/s free-stream velocity has a higher C_p than the lower free-stream velocities. This difference in C_p is attributed to the extent of the flow separation encountered at the high free-stream velocity; as well, as previously discussed, the non-uniformities in the flow after the 1st elbow were extreme and could not be completely eliminated by the solid honeycomb. However, the solid honeycomb was able to generate enough uniform flow at the high free-stream velocity to remove the constant C_p that occurred in the baseline flow. The constant C_p signified that no acceleration or deceleration of the flow occurred due to the extent of flow separation.

In the exit section of the duct, the trend is very similar to the baseline, however as discussed previously, the exit section also benefits from the solid honeycomb installed after the 1st elbow because the more uniform flow entering the 2nd elbow translates into a more uniform flow entering the exit section. A more uniform flow has a higher local velocity and lower C_p.

As discussed in the results along the 0° wall of the exit section, the high value of C_p at the 100ft/s free-stream velocity is a result of the extent of flow separation that occurs in the elbows. The non-uniformities from the 1st elbow that were not completely eliminated by the solid honeycomb coupled with the non-uniformities of the 2nd elbow translate into a highly non-uniform exit flow with low local velocities and high static pressures.

Although the solid honeycomb significantly reduced the non-uniformities, variations in C_p still exist as the flow moves downstream. This indicates that fully uniform flow has not been achieved by the end of the measurement region.

Pressure Results Along 270 °Azimuth Angle

The inlet section shows no additional upstream effects, Figure 4-20d, generated by the solid honeycomb, except at the high free-stream velocity tested. The upstream effects are indicated by the variations in C_p. The upstream effects generated by the honeycomb are more dominant with the high-energy flow. Because the high-energy flow is traveling at a high velocity, when it encounters the honeycomb it then changes its path drastically forcing the upstream flow to respond. The C_p values at the lower free-stream velocities yield the same results as the baseline.

The same trend as the baseline is exhibited in the 2nd elbow, Figure 4-20c, however the values of C_p with the solid honeycomb installed are lower. As discussed previously, the honeycomb helps to reduce pipe swirl and non-uniformities generated by the flow separation in the 1st elbow by redistributing the flow. This reduction enables the flow entering the 2nd elbow to be more uniform. A more uniform flow translates into a higher local velocity and lower C_p entering the 2nd elbow.

As the flow moves into the exit section of the duct, the C_p trends between the baseline and the solid honeycomb are the same, Figure 4-20c. The solid honeycomb helps to generate a more uniform flow entering the 2nd elbow and the exit section, resulting in a lower C_p and a higher local velocity. The 2nd elbow however, generates non-uniformities of its own as a result of the flow separation and the existence of secondary flow. By the end of the measurement region, flow uniformity has not been fully achieved and results obtained are similar to those discussed in the flow along the 0° wall of the exit section. Since the variations in C_p, which signify a non-uniform flow, are diminishing, it is anticipated that flow uniformity will be achieved slightly further downstream in the exit section.

4.2.2.2 20% Porous-Cell Honeycomb Pressure Results

Non-dimensional pressure distributions, for the 20% porous-cell honeycomb located after the 1st elbow, along the ducts 3 azimuth angles of 0°, 180°, and 270° and for the free-stream velocities of 60ft/s, 80ft/s, and 100ft/s are shown in Figures 4-21a, 4-21b, 4-21c, and 4-21d.

Pressure Results Along 0° Azimuth Angle

The trend, Figure 4-21a, for all 3 free-stream velocities tested, is the same as that obtained with the solid honeycomb, Figure 4-20a. The values of C_p in the exit section of the duct are significantly lower than the baseline results.

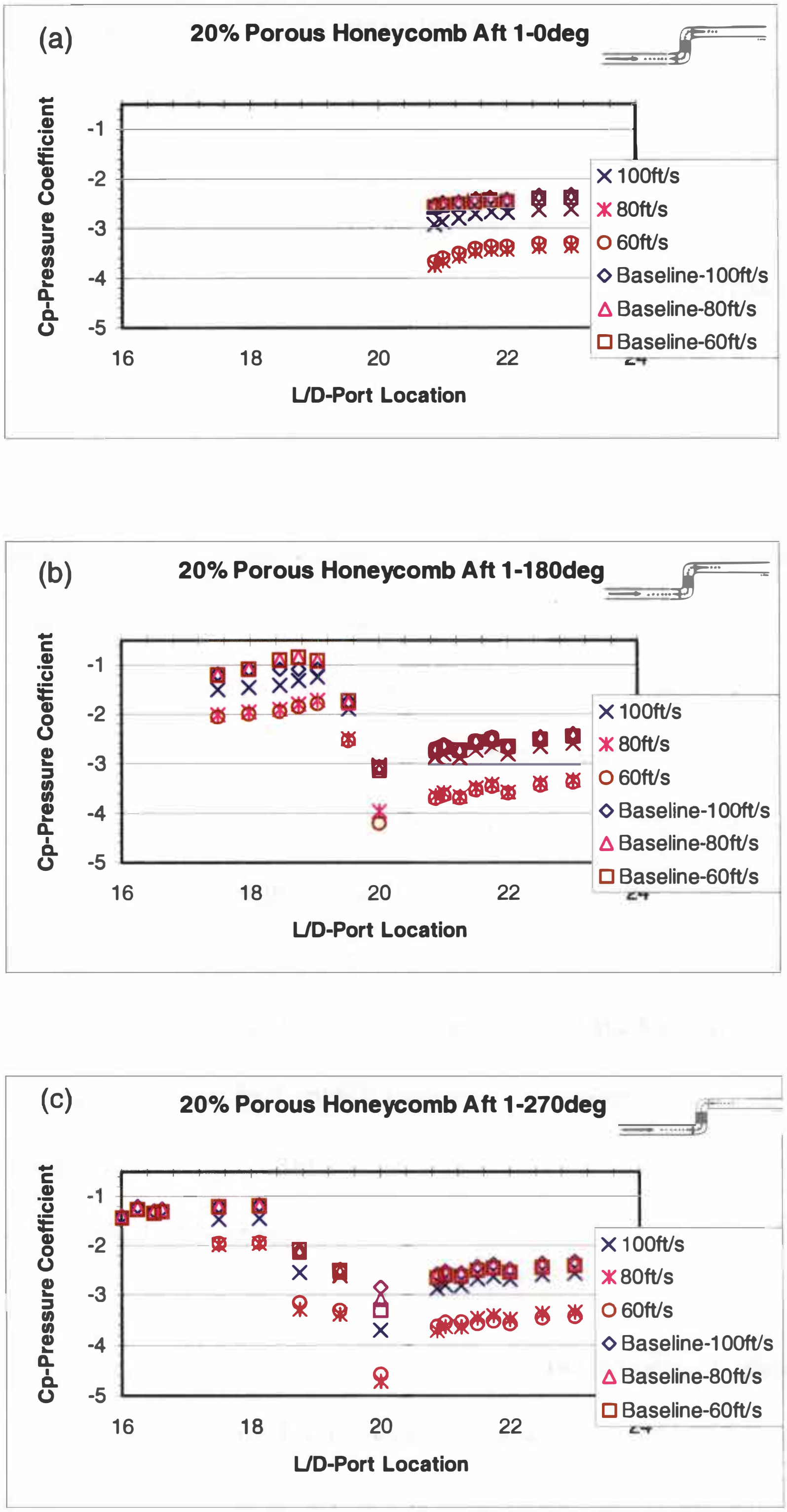

Figure 4-21. C_p vs. L/D-20% Porous-Cell Honeycomb Aft 1st Elbow

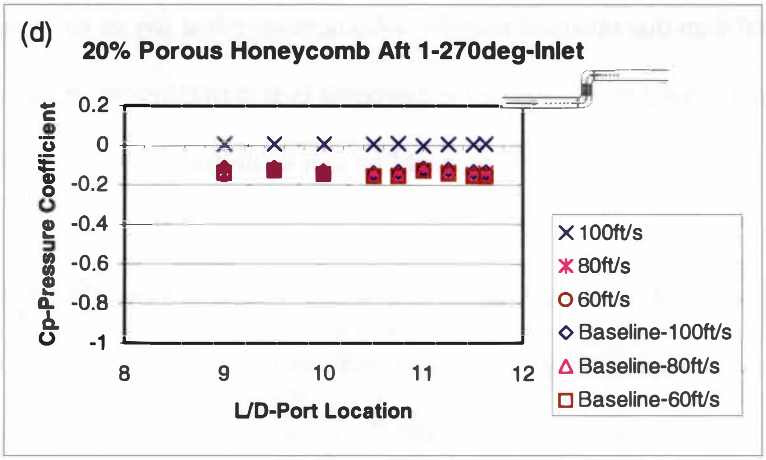

Figure 4-21. Cont'd

The values of C_p are also slightly lower than those obtained when the solid honeycomb is installed after the 1st elbow. Variations in C_p exist as the flow recovers from the non-uniformities generated by secondary flow and separated flow in the 2nd elbow. Near the end of the pressure measurements region, the flow non-uniformities have significantly decreased and the flow establishes a more uniform flow. This signifies that the 20% porous-cells help to reduce not only the lateral disturbances but the axial disturbances as well. The non-porous cells perform their traditional role of eliminating any remaining lateral disturbances in the flow generated by the flow separation and the existence of secondary flow in the 1st elbow, as well as eliminating any disturbances generated by flow passing between adjacent cells (in the porous section of the honeycomb).

Pressure Results Along 180 °Azimuth Angle

Measurements indicate, Figure 4-21b, that the C_p values throughout the measurement section for all 3 free-stream velocities tested are lower than those obtained for the baseline. The trend exhibited in Figure 4-21b is also very similar to the trend exhibited by the solid honeycomb in Figure 4-20b; however the increase in C_p as the flow moves through the elbow is more gradual than that obtained with the solid honeycomb at any of the free-stream velocities tested. The 20% porous-cell honeycomb is able to eliminate more of the axial and lateral disturbances from the 1st elbow, enabling a more uniform flow to travel through the 2nd elbow.

Although the flow is more uniform as it enters the 2nd elbow, flow separation still affects the flow as illustrated by the last measurement taken as the flow leaves the elbow. The different C_p values are an indication that the region of flow separation has moved further downstream.

In the exit section of the duct, the increase in C_p as the flow tries to recover from the 2nd elbow is also more gradual than that exhibited in Figure 4-20b by the solid honeycomb, Sec 4.2.2.1. The C_p in the exit section of the duct displays fewer pressure and velocity variations as the flow moves downstream, the reasons for this improved flow is attributed to the upstream history of the flow. The porous holes in the honeycomb act as flow passages between cells. The holes in each cell wall enable the total pressure to balance between adjacent cells, thus averaging the total pressure between adjacent cells. The averaging of the total pressure helps to reduce axial and lateral disturbances in the porous section, while the non-porous section further eliminates any remaining lateral disturbances in the flow. This results in a more uniform flow traveling into the 2nd elbow. A more uniform flow has a higher local velocity and lower static pressure traveling through the 2nd elbow and into the exit section of the duct.

The results illustrate that the 20% porous-cell honeycomb establishes a more uniform flow entering the 2nd elbow and the exit section of the duct. A more uniform flow results in a higher local velocity and lower C_p.

Pressure Results Along 270° Azimuth Angle

Measurements indicate, Figure 4-21d, that no additional upstream effects occur in the inlet section as a result of the 20% porous-cell honeycomb located after the 1st elbow.

In the 2nd elbow, Figure 4-21c, the 20% porous-cell honeycomb has the same effect as the solid honeycomb, Figure 4-20c, in lowering the values of C_p. No significant differences exist between the 2 configurations with respect to the trend or values of C_p.

Similarly in the exit section of the duct, the 20% porous-cell honeycomb results in a slightly larger decrease in C_p than the solid honeycomb. The flow, particularly at the 60ft/s free-stream velocity, has fewer variations in C_p indicating a more uniform flow within a shorter exit section.

Overall, the 20% porous-cell honeycomb achieved a greater result than the solid honeycomb in establishing a more uniform flow as the flow moves through the 2nd elbow and into the exit section. The 20% porous-cell honeycomb decreased the C_p significantly over the baseline results, particularly at the 2 lower free-stream velocities tested.

4.2.2.3 30% Porous-Cell Honeycomb Pressure Results

Non-dimensional pressure distributions, for the 30% porous-cell honeycomb located after the 1st elbow, along the ducts 3 azimuth angles of 0°, 180°, and 270° and for the free-stream velocities of 60ft/s, 80ft/s, and 100ft/s are shown in Figures 4-22a, 4-22b, 4-22c, and 4-22d.

Pressure Results Along 0° Azimuth Angle

The trend, Figure 4-22a, is very similar to that obtained with the solid honeycomb and the 20% porous-cell honeycomb installed, Sec 4.2.2.1 and 4.2.2.2.

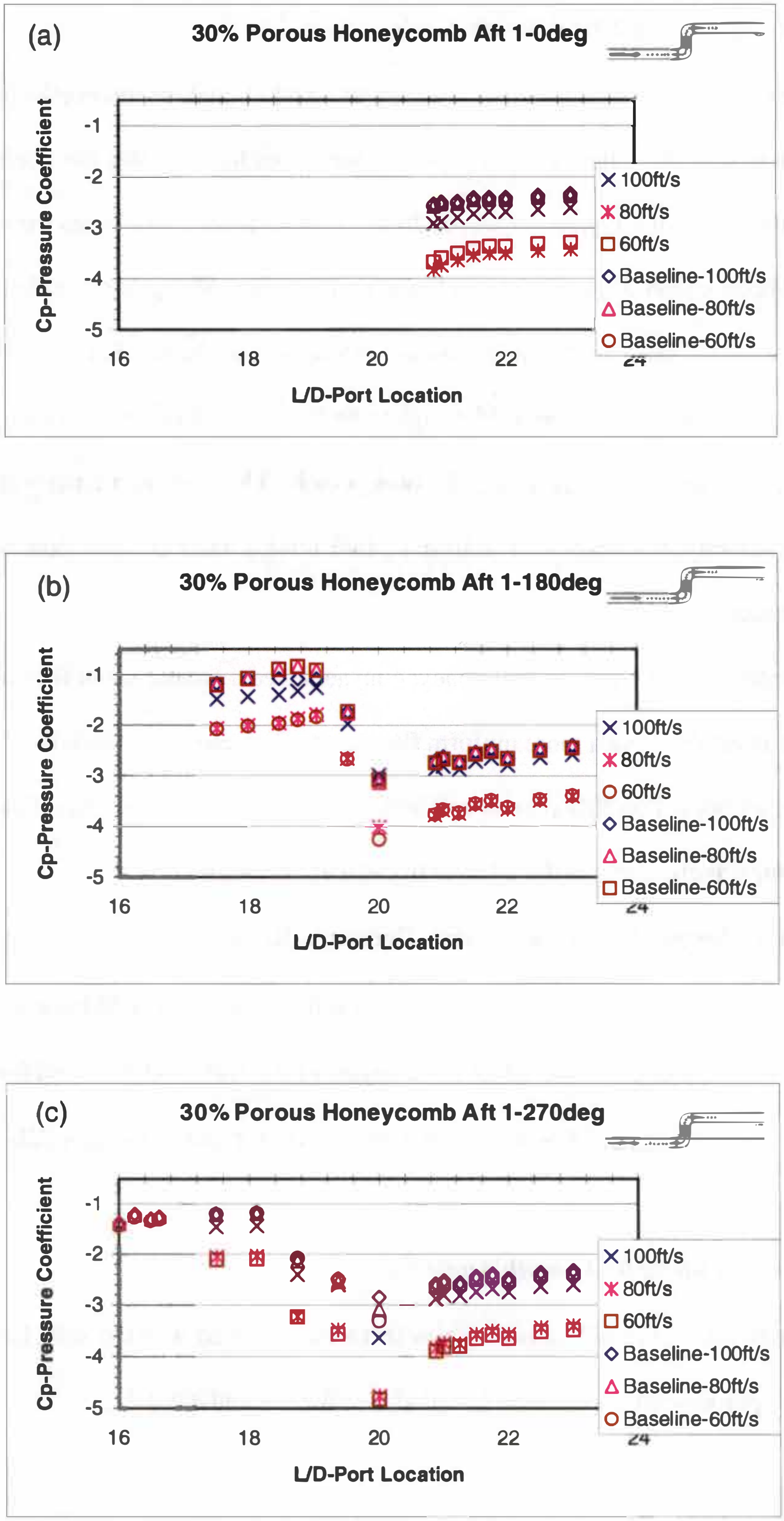

Figure 4-22. C_p vs. L/D-30% Porous-Cell Honeycomb Aft 1st Elbow

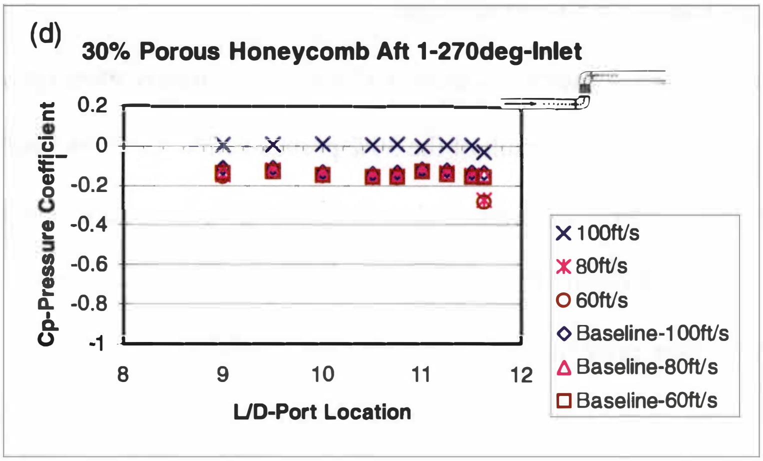

Figure 4-22. Cont'd

Interestingly however, at the 60ft/s and 100ft/s free-stream velocities tested, the values of C_p obtained with the 30% porous-cell honeycomb do not vary from those obtained with the 20% porous-cell honeycomb. The 80ft/s free-stream velocity exhibits a noticeable decrease in C_p. This is an interesting trend since it was expected that all free-stream velocities would experience a slight decrease in C_p. The flow that is measured along this wall in the exit duct is separated flow. The results indicate that along the 0° wall of the 2nd elbow, the region of flow separation at the high and low free-stream velocities tested with the 20% or 30% porous-cell honeycomb installed, are very similar.

Pressure Results Along 180° Azimuth Angle

The 30% porous-cell honeycomb, Figure 4-22b, generates a similar trend as the 20% porous-cell honeycomb, Figure 4-21b, along the 180° wall in both the 2nd elbow and the exit section of the duct, Sec 4.2.2.2. The 30% porous-cell honeycomb generates a more uniform flow traveling into the 2nd elbow however, resulting in slightly lower values of C_p in the 2nd elbow and the exit section of the duct.

Pressure Results Along 270° Azimuth Angle

The inlet section of the duct, Figure 4-22d, exhibits slightly more upstream effects (than previously exhibited) as a result of the 30% porous-cell honeycomb located after the 1st elbow. The upstream effects are more evident at the 100ft/s free-stream velocity tested, Sec 4.2.2.1. Figure 4-22d illustrates that more variations in C_p exist and as a result slightly more swirl occurs in the flow prior to the flow entering the 1st elbow.

The flow moving through the 2nd elbow, Figure 4-22c, exhibits the same trend as that obtained with the solid honeycomb, Sec 4.2.2.1, and the 20% porous-cell honeycomb, Sec 4.2.2.2, however the values of C_p are lower, particularly at the 2 lower free-stream velocities tested. This indicates that the 30% porous-cell honeycomb generates a slightly more uniform flow, with a higher local velocity and lower C_p as the flow enters the 2nd elbow. At the 100ft/s free-stream velocity tested, the 30% porous-cell honeycomb is no more effective than the solid honeycomb or the 20% porous-cell honeycomb in achieving a uniform flow prior to entering the 2nd elbow. The same values of C_p along the duct elbow at the 100ft/s free-stream velocity iterates the conclusion that flow separation in the 1st elbow was so extensive that the additional porosity of the honeycomb was unable to generate an improved flow.

In the exit section, the values of C_p are slightly lower than those obtained with the 20% porous-cell honeycomb at all free-stream velocities tested, however the flow exhibits slightly more variations in C_p than those exhibited with the 20% porous-cell honeycomb. With more porous cells, the flow exchange between adjacent cells may have generated some additional disturbances prior to entering the 2nd elbow. Uniformity is achieved, however within the same distance downstream with the 30% porous-cell honeycomb as was obtained with the 20% porous-cell honeycomb.

Overall, the 30% porous-cell honeycomb was successful in achieving a slightly more uniform flow entering the 2nd elbow, with a slightly lower C_p and a slightly higher local velocity compared to the 20% porous-cell honeycomb. These decreases in C_p however, are not significant.

4.2.2.4 40% Porous-Cell Honeycomb Pressure Results

Non-dimensional pressure distributions, for the 40% porous-cell honeycomb located after the 1st elbow, along the ducts 3 azimuth angles of 0°, 180°, and 270° and for the free-stream velocities of 60ft/s, 80ft/s, and 100ft/s are shown in Figures 4-23a, 4-23b, 4-23c, and 4-23d.

Pressure Results Along 0° Azimuth Angle

Measurements indicate, Figure 4-23a, that the 40% porous-cell honeycomb is very effective in redistributing the non-uniformities generated by flow separation and secondary flow from the 1st elbow. These trends, Figure 4-23a, are similar to those displayed with the other honeycombs, particularly the 20% porous-cell honeycomb, Sec 4.2.2.2. The values of C_p are lower, for all free-stream velocities tested, than the baseline values, as well as, for any other honeycomb tested. Fewer variations in C_p at all free-stream velocities tested also exist as the flow moves downstream in the exit duct, indicating a more uniform flow towards the end of the pressure measurements region.

Pressure Results Along 180° Azimuth Angle

The results obtained with the 40% porous-cell honeycomb installed, Figure 4-23b, are very similar to the previous discussions (20% porous-cell honeycomb) as the flow moves through the elbow, Sec 4.2.2.2. With the presence of a more porous-cell honeycomb the increase in C_p as the flow moves through the elbow becomes more gradual indicating fewer losses as a result of the flow separation in the elbow. The flow is able to leave the elbow and move into the exit section with a higher local velocity.

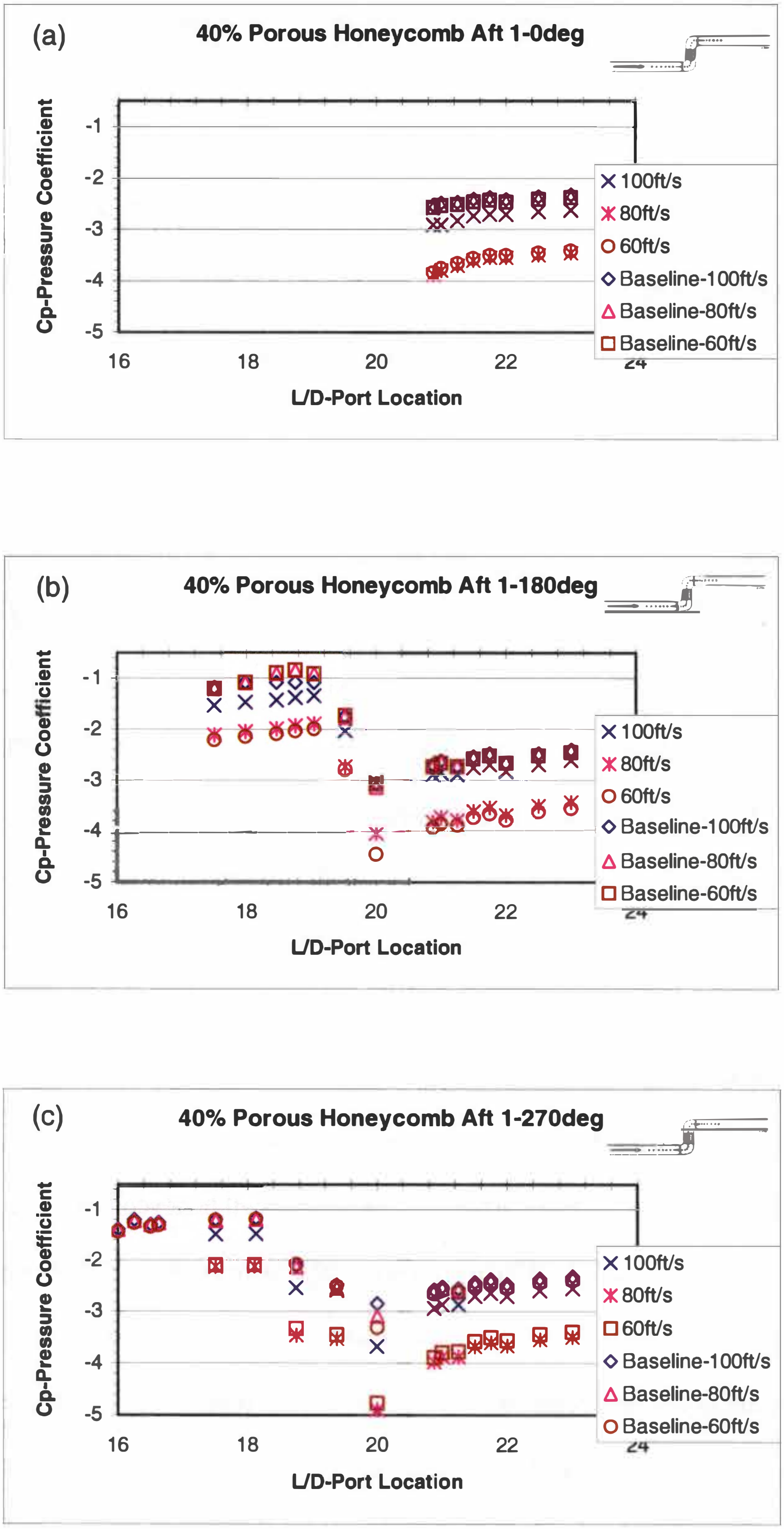

Figure 4-23. C_p vs. L/D-40% Porous-Cell Honeycomb Aft 1st Elbow

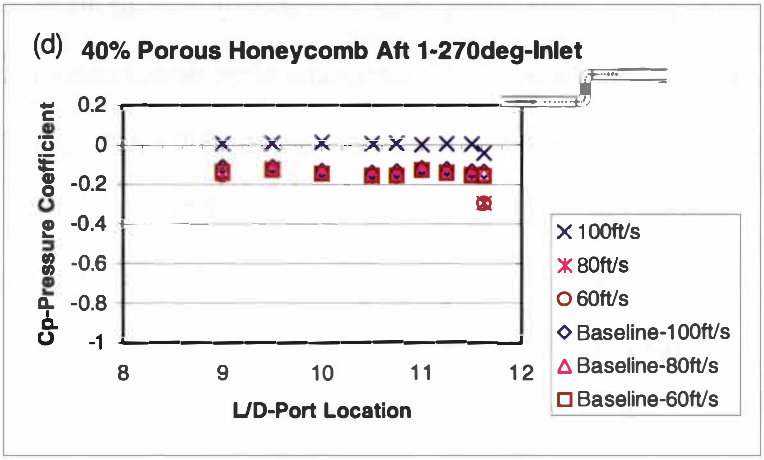

Figure 4-23. Cont'd

The C_p values obtained in the exit section are again lower than those obtained with other honeycombs installed. Variations in C_p are present as the flow moves in the exit section, Figure 4-23b. Similar to the previous discussions along the 180° wall in the exit section of the duct, Sec 4.2.2.2, as the flow moves downstream, the variations in C_p diminish.

Pressure Results Along 270° Azimuth Angle

The inlet section of the duct, Figure 4-23d, exhibits the same results as those obtained with the 30% porous-cell honeycomb installed, Sec 4.2.2.3. Similar upstream effects generated by the 40% porous-cell honeycomb exist at all free-stream velocities, causing the flow to swirl prior to entering the 1st elbow.

The flow moving through the 2nd elbow, Figure 4-23c, also displays a similar trend as the previous honeycomb. The 40% porous-cell honeycomb decreases the C_p values slightly more than the other honeycombs along the elbow, particularly at the lower free-stream velocity tested. At the high free-stream velocity, very little change exists compared to the other honeycombs installed, Sec 4.2.2.3.

As the flow moves into the exit section, interestingly only the 80ft/s free-stream velocity experiences a slight decrease in C_p (at the end of the measurement region) from values obtained with the 30% porous-cell honeycomb. The 60ft/s and 100ft/s free-stream velocities tested actually experience a slight increase in C_p (40% porous-cell honeycomb) from the values obtained with the 30% porous-cell honeycomb. This is attributed to the larger percent porosity honeycomb generating additional disturbances as the flow moves between adjacent cells. As well, at the high free-stream velocity, the additional porosity is not effective in removing the significant disturbances generated by the elbows. Flow uniformity has not been fully achieved by the end of the measurement region, however variations in C_p have diminished, indicating flow uniformity will be achieved shortly downstream.

Overall, the results indicate that the honeycombs when installed after the 1st elbow redistribute the non-uniform flow generated by flow separation and the secondary flow in the 1st elbow. The flow entering the 2nd elbow is then more uniform with a higher local velocity and lower static pressure. The more uniform flow traveling through the 2nd elbow generates a more uniform flow with a higher local velocity entering the exit section of the duct.

At high free-stream velocities however, flow separation in the 1st elbow is very large. With a highly non-uniform flow, the more porous honeycomb is not very effective in establishing a more uniform flow, Figure 4-24a.

Figures 4-24(a-c) illustrate the average C_p at each location in the exit section of the duct, this gives a reasonable indication of flow uniformity throughout the exit duct with the honeycombs installed. Although all the honeycombs achieved improved results over baseline values, the 40% porous-cell honeycomb achieved the best results in terms of lowering the C_p in most areas of the duct.

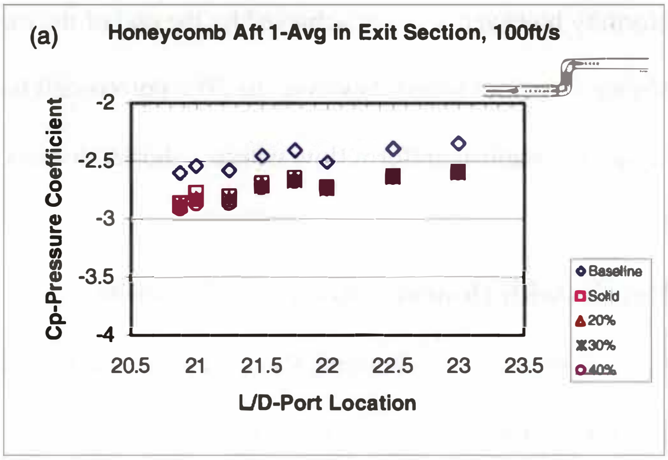

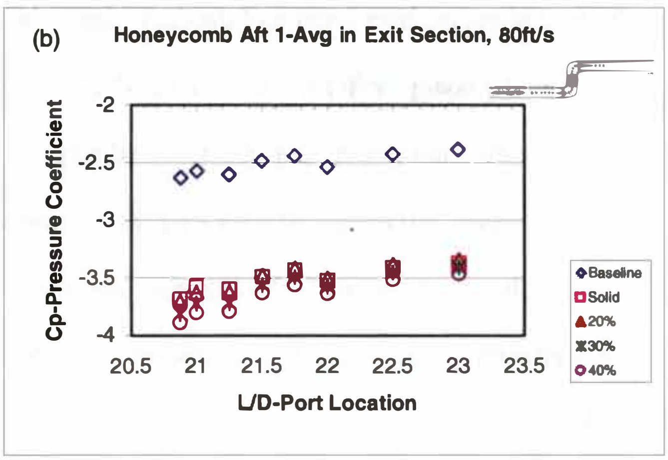

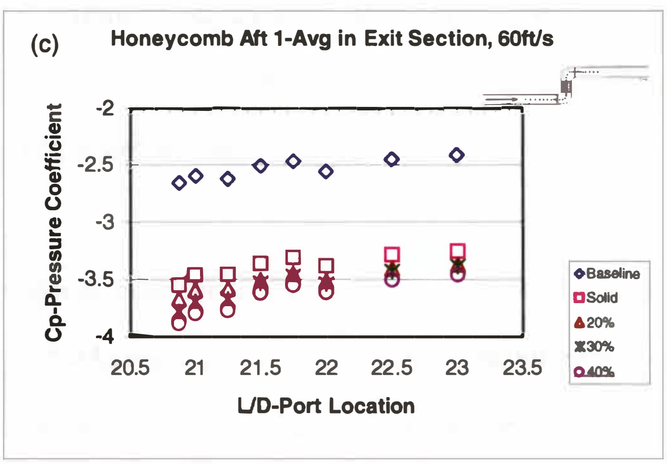

Figure 4-24. Honeycomb Aft 1st Elbow, Average C_p in Exit Duct

Complete flow uniformity however, was not achieved by the end of the measurement region at any of the free-stream velocities tested; however the 20% porous-cell honeycomb achieved the best results in trying to establish uniform flow within a shorter distance downstream of the 2^{nd} elbow.

4.2.3 Pressure Results with Honeycombs After 2^{nd} Elbow

Non-dimensional pressure distributions, for the honeycomb located after the 2^{nd} elbow, along the duct for 3 azimuth angles of 0°, 180°, and 270°, and for 3 free-stream velocities of 60ft/s, 80ft/s, and 100ft/s are discussed in the following sections. No pressure measurements were obtained along the inlet section of the duct. Since the upstream effects in the inlet section, generated by the honeycomb located after the 1^{st} elbow, did not affect the flow significantly, it was assumed that no upstream effects would be generated in the inlet section with the honeycomb located further downstream after the 2^{nd} elbow. The focus was on measurements obtained in the 2^{nd} elbow and in the exit duct after the honeycomb to evaluate the honeycomb's effect in generating a more uniform flow within a shorter distance downstream in the exit duct.

4.2.3.1 Solid Honeycomb Pressure Results

Non-dimensional pressure distributions, for the solid honeycomb located after the 2^{nd} elbow, along the duct for 3 azimuth angles of 0°, 180°, and 270° and for 3 free-stream velocities of 60ft/s, 80ft/s, and 100ft/s are shown in Figures 4-25a, 4-25b, and 4-25c.

Pressure Results Along 0° Azimuth Angle

Measurements indicate, Figure 4-25a, that with the solid honeycomb located after the 2^{nd} elbow, the C_p decreases for all free-stream velocities compared to baseline values in the exit section of the duct. The reduction in C_p signifies a higher local velocity than that of the baseline as the flow moves downstream.

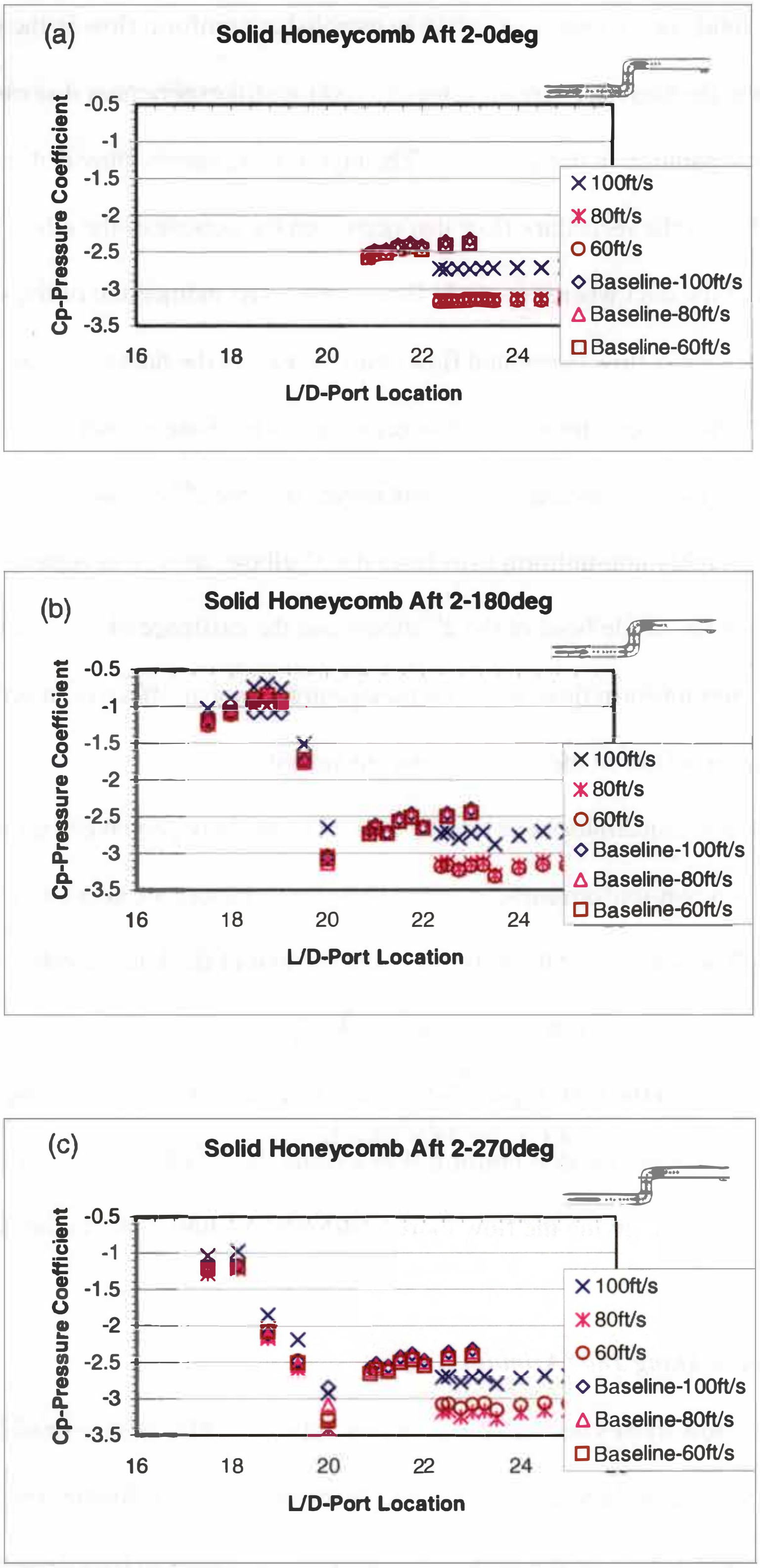

Figure 4-25. C_p vs. L/D-Solid Honeycomb Aft 2nd Elbow

Although the solid honeycomb is effective in establishing uniform flow in the exit section of the duct, flow at the high free-stream velocity, 100ft/s, still experiences disturbances from the extent of flow separation in the 1st elbow. The high kinetic energy flow that moves through the 1st elbow forces the secondary flow that occurs on the outside of the elbow to the far opposite wall of the duct where separated flow exists. The momentum of the secondary flow pushes the low energy flow (separated flow) into the exit of the duct elbow and into the 6-inch connector duct. Since the 6-inch connector duct is not long enough to establish uniformity in the flow, the non-uniform flow moves into the 2nd elbow. As a result, the 2nd elbow contains highly non-uniform flow from the 1st elbow, as well as separated flow originating from the inside bend of the 2nd elbow and the existence of its own secondary flow. With a highly non-uniform flow, the solid honeycomb is not as effective in achieving a completely uniform flow at the high free-stream velocity.

Slight non-uniformities exist as the flow exits the honeycomb cells; the honeycomb generates its own non-uniformities, however these disturbances are small and dissipate quickly. The flow achieves uniformity very near the exit of the honeycomb. At L/D of 24.1, the flow has become uniform with no variations in C_p.

The points on the plot, Figure 4-25a, have near zero slopes, indicating that the solid honeycomb redistributes the non-uniform flow exiting the 2nd elbow. The redistribution of flow reduces the swirl, giving the flow more uniformity, resulting in a higher local velocity and a lower C_p.

Pressure Results Along 180° Azimuth Angle

As the flow moves through the 2nd elbow, upstream effects generated by the solid honeycomb are evident, Figure 4-25b. At the lower free-stream velocities the C_p values are slightly lower than their baseline values, signifying fewer losses in the elbow and a slightly higher local velocity. At the high free-stream velocity, the upstream effects are more significant and have the opposite effect. The value of C_p is higher than the baseline as the flow moves through the bend, signifying more losses and lower local velocities. At the same time however, the solid honeycomb eliminates the large area of flow separation encountered in the baseline indicated by the constant C_p. As previously discussed, the constant C_p in this region signifies that no acceleration or deceleration of the flow occurs due to the extent of flow separation. The 100ft/s free-stream velocity entering the 2nd elbow is a high energy flow, the upstream effect of the honeycomb is that some of the energy is utilized to eliminate the large area of flow separation that encompasses the 2nd elbow, as a result, the local flow velocity is lower and the C_p higher.

As the flow moves into the exit section, the solid honeycomb helps to redistribute the non-uniformities generated in the elbows and establishes a more uniform flow with a higher local velocity and fewer losses than the baseline. A difference in C_p still exists between the high free-stream velocity and the lower free-stream velocities. This difference signifies that the solid honeycomb is able to generate a more uniform flow, but is still not as effective in eliminating all the non-uniformities in the flow at the high free-stream velocity. This is a result of the extent of flow separation that occurs in the elbows experienced by the high free-stream velocity. As previously discussed, the high kinetic energy flow forces the non-uniformities from the 1st elbow further into the 6-inch connector duct. As a result, a highly non-uniform flow enters the 2nd elbow. The oncoming non-uniform flow coupled with the existence of secondary flow and separated flow from the 2nd elbow generates a highly non-uniform flow with significant axial and lateral disturbances, which the solid honeycomb is unable to completely eliminate.

Compared to baseline results however, all free-stream velocities exhibit a noticeable decrease in C_p. There are also fewer losses as the flow leaves the solid honeycomb and enters the exit duct. Uniform flow is achieved, with no variations in C_p, at L/D of 24.4, for all free-stream velocities tested.

Pressure Results Along 270° Azimuth Angle

Similarly in this orientation, Figure 4-25c, upstream effects from the solid honeycomb are more evident particularly at the 80ft/s and 100ft/s free-stream velocities. At 80ft/s free-stream velocity, the C_p decreases from its baseline value resulting in a higher local velocity as the flow moves through the elbow. At 100ft/s free-stream velocity, the C_p increases from its baseline value resulting in a lower local velocity as the flow moves through the elbow. As previously discussed, the high-energy flow is used to eliminate the large area of flow separation; this results in an increase in C_p and a lower local velocity.

As the flow exits the 2nd elbow and moves through the solid honeycomb and into the exit section, the C_p decreases from the baseline results for all free-stream velocities. The non-uniformities that still exist are very small, and within a short distance downstream of the exit section of the honeycomb, the flow establishes uniformity. Flow uniformity is achieved at L/D of 24.3.

In all 3 orientations, the solid honeycomb has a beneficial effect in establishing a more uniform flow in the exit section of the duct. To have a fully uniform duct flow however, the C_p must be the same in all orientations. By comparing the values of L/D, the extent of flow uniformity is determined. With the solid honeycomb, fully uniform duct flow is established at L/D of 24.2.

4.2.3.2 20% Porous-Cell Honeycomb Pressure Results

Non-dimensional pressure distributions, for the 20% porous-cell honeycomb located after the 2nd elbow, along the duct for 3 azimuth angles of 0°, 180°, and 270° and for the free-stream velocities of 60ft/s, 80ft/s, and 100ft/s are illustrated in Figures 4-26a, 4-26b, and 4-26c.

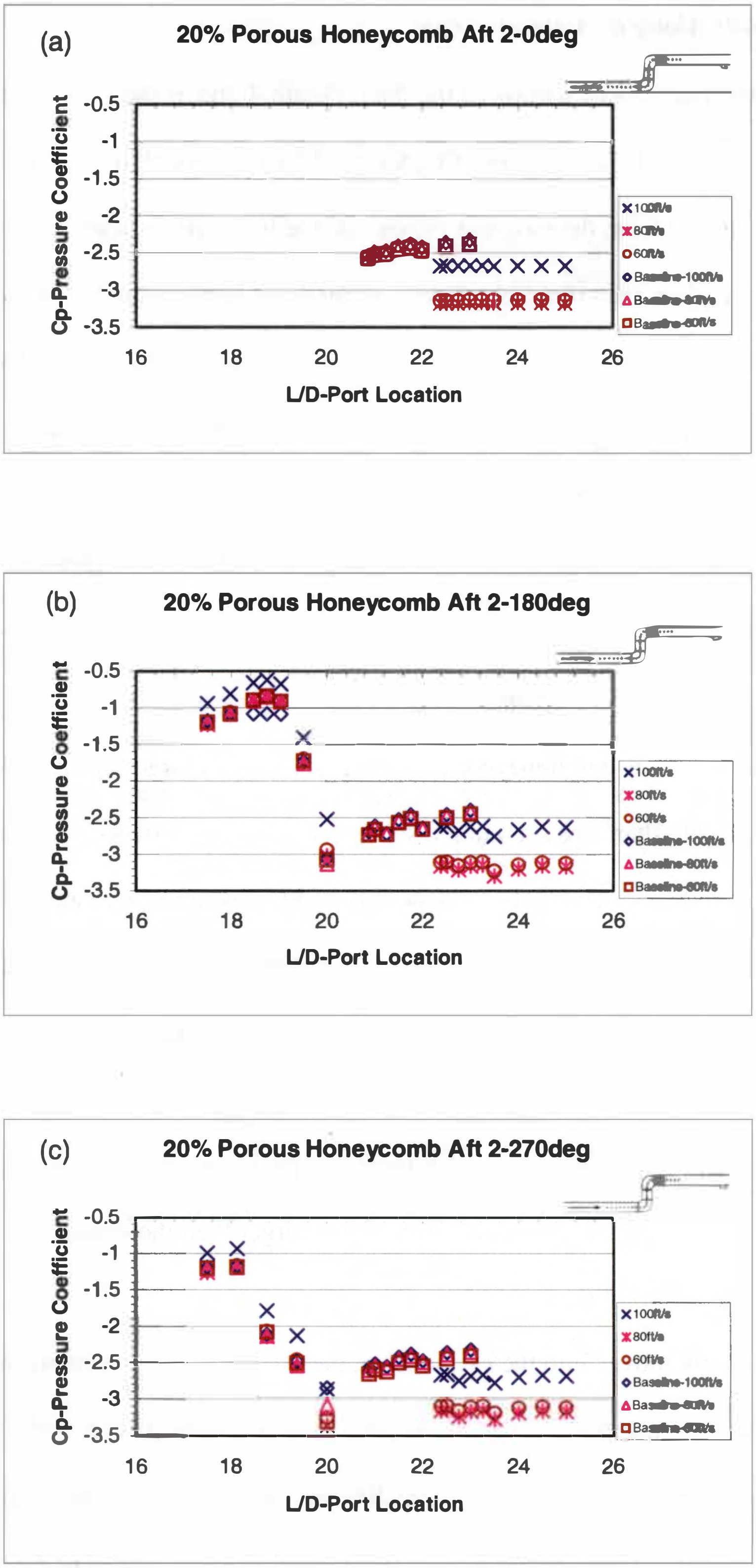

Figure 4-26. C_p vs. L/D-20% Porous-Cell Honeycomb Aft 2nd Elbow

Pressure Results Along 0° Azimuth Angle

The trend in the exit section of the duct, Figure 4-26a, is the same as that of the solid honeycomb, Sec 4.2.3.1. The values of C_p for the 20% porous-cell honeycomb are significantly reduced from the baseline values. At the lower free-stream velocities the C_p values are slightly less than those obtained with the solid honeycomb but at the 100ft/s free-stream velocity the values of C_p, as the flow leaves the honeycomb, are slightly more than those obtained with the solid honeycomb. However, there are fewer C_p variations with the 20% porous-cell honeycomb indicating that the 20% porous-cell honeycomb helps to eliminate more of the non-uniformities generated in the elbows. The flow becomes fully uniform at L/D of 23.5.

Pressure Results Along 180° Azimuth Angle

The 20% porous-cell honeycomb generates a slightly larger upstream effect in the elbow, Figure 4-26b, than was seen in the solid honeycomb, Figure 4-25b, Sec 4.2.3.1. At the lower free-stream velocities, the 20% porous-cell honeycomb generates a slight upstream effect predominantly at the point closest to the exit of the bend; the C_p increases slightly compared to the baseline value. The most evident upstream effect is at the high free-stream velocity tested, the trend is very similar to that obtained with the solid honeycomb, Sec 4.2.3.1. The 20% porous-cell honeycomb increases the C_p resulting in a lower local velocity along the bend, Sec 4.2.3.1. These values of C_p are larger than those generated by the upstream effects of the solid honeycomb.

As the flow moves into the exit section, the 20% porous-cell honeycomb is effective in reducing the non-uniformities in the flow, and a similar trend is seen as the one produced with the solid honeycomb, Sec 4.2.3.1. The 20% porous-cell honeycomb exhibits fewer variations between C_p values as the flow moves downstream compared to the solid honeycomb. The porous-cell honeycomb generates a more uniform flow because both axial and lateral disturbances are reduced. The flow achieves fully uniform flow, recovering from the slight disturbances generated from the exit of the honeycomb at L/D of 23.8.

Pressure Results Along 270° Azimuth Angle

The trend and results, Figure 4-26c, obtained in the 2nd elbow and in the exit section are the same as those obtained with the solid honeycomb, Sec 4.2.3.1.

In the exit section, the 20% porous-cell honeycomb is effective in reducing the axial and lateral disturbances in the flow and as a result decreases the values of C_p from the baseline values. The 20% porous-cell honeycomb is also more effective than the solid honeycomb in reducing the non-uniformities generated by the elbows and in establishing a more uniform flow. This is evident by the decrease in C_p variations in the exit section of the duct. The 20% porous-cell honeycomb achieves flow uniformity within a short distance downstream of the exit section of the honeycomb, at L/D of 24.

The overall results obtained for the 20% porous-cell honeycomb showed slight improvements in the results when compared to the solid honeycomb. Although the solid honeycomb and 20% porous-cell honeycomb were equally effective in reducing the non-uniformities generated by the 2nd elbow as illustrated by the decrease in C_p, the 20% porous-cell honeycomb was more effective in achieving a more uniform flow within a shorter distance downstream of the honeycomb exit. Fully uniform duct flow was achieved at L/D of 24.

4.2.3.3 30% Porous-Cell Honeycomb Pressure Results

Non-dimensional pressure distributions, for the 30% porous-cell honeycomb installed after the 2nd elbow, along the duct of 3 azimuth angles of 0°, 180°, and 270° and for the free-stream velocities of 60ft/s, 80ft/s, and 100ft/s are shown in Figures 4-27a, 4-27b, and 4-27c.

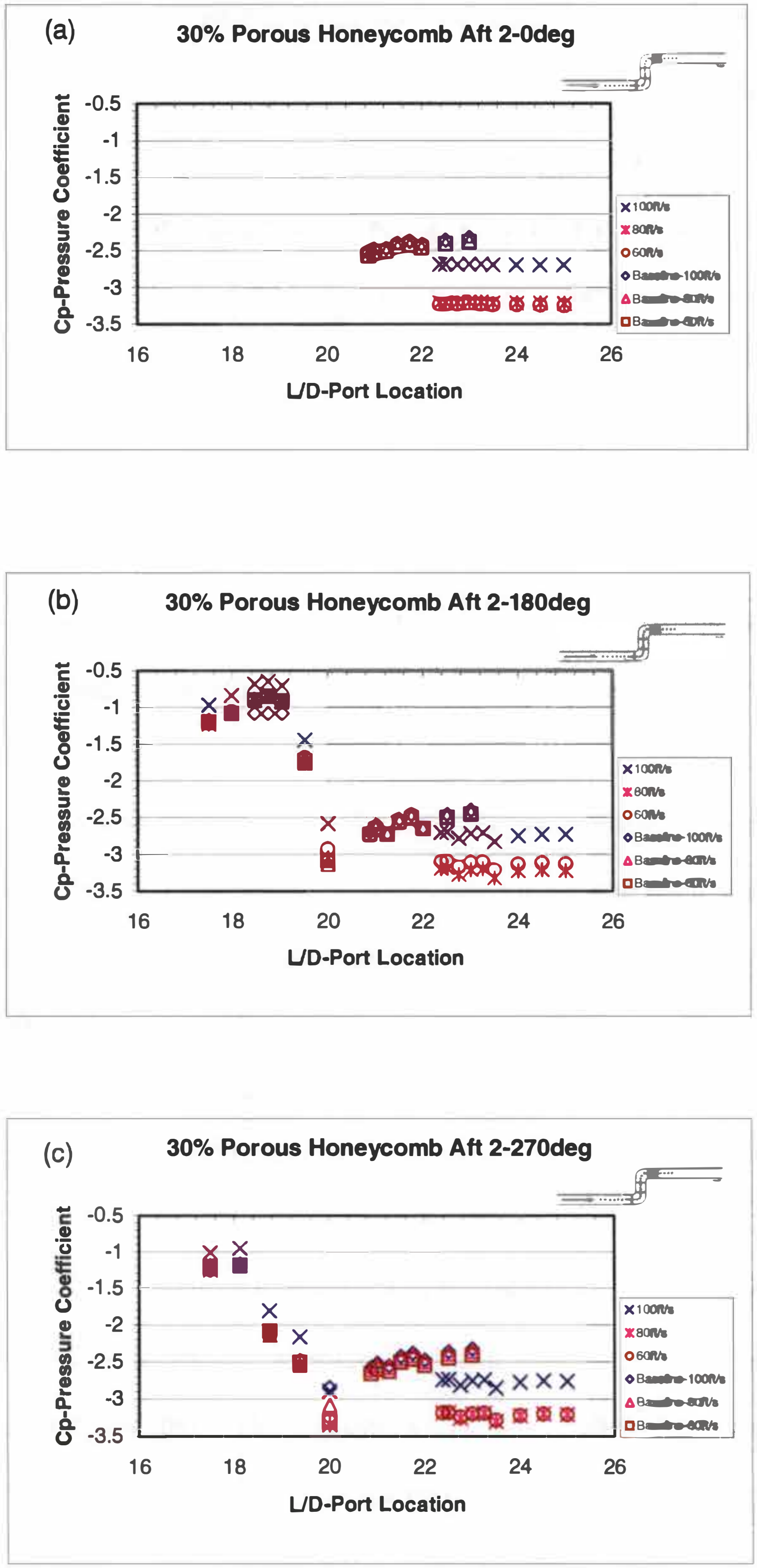

Figure 4-27. C_p vs. L/D-30% Porous-Cell Honeycomb Aft 2nd Elbow

Pressure Results Along 0° Azimuth Angle

Similar to the solid and 20% porous-cell honeycomb, Sec 4.2.3.1 and 4.2.3.2, the 30% porous-cell honeycomb, Figure 4-27a, establishes a more uniform flow in the exit section of the duct. The C_p for all free-stream velocities tested is significantly lower than the baseline results. At the lower free-stream velocities tested, the 30% porous-cell honeycomb also decreases the C_p significantly from the values obtained with the 20% porous-cell honeycomb. The 100ft/s free-stream velocity exhibits no change with a more porous honeycomb installed. As previously discussed, along the 0° wall of the duct, the flow passing through this section of the honeycomb is separated flow, at 100ft/s free-stream velocity the flow separation is extreme, so the additional porosity in eliminating the non-uniformities is ineffective. The flow pattern, as observed from the surface oil flow visualization in the exit section, Figure 4-16 illustrates that the flow after the 30% porous-cell honeycomb is very uniform with very little swirl. The flow becomes fully uniform in the exit section at L/D of 23.5.

Pressure Results Along 180° Azimuth Angle

The 30% porous-cell honeycomb, Figure 4-27b, generates the same upstream effects in the elbow at the high free-stream velocity as those produced by the 20% porous-cell honeycomb, Sec 4.2.3.2.

As the flow moves into the exit section, the 30% porous-cell honeycomb decreases the C_p values at the 80ft/s and 100ft/s free-stream velocities. At 60ft/s free-stream velocity very little change from the 20% porous-cell honeycomb results is seen. From the surface oil flow visualization results, Figure 4-15, the flow patterns illustrate a swirl in the flow leaving the 30% porous-cell honeycomb. The C_p exhibits slight variations in the initial exit of the honeycomb but within a short distance becomes more linear compared to its baseline values signifying a more uniform flow. This occurs at an L/D of 23.8.

Pressure Results Along 270° Azimuth Angle

The upstream effects in the elbow generated by the 30% porous-cell honeycomb, Figure 4-27c, are evident at the high free-stream velocity tested and are the same as those of the 20% porous-cell honeycomb, Sec 4.2.3.2.

In the exit section, the 30% porous-cell honeycomb has helped to establish a more uniform flow with fewer losses in the exit section. This is illustrated with the decrease in C_p values from the baseline results. The trend is very similar to that obtained with the 20% porous-cell honeycomb, Sec 4.2.3.2, however the values of C_p are slightly lower and the flow establishes uniformity at L/D of 23.9.

Overall, the 30% porous-cell honeycomb helped to establish a more uniform flow with minimal losses in the exit section of the duct. Flow uniformity was greatly improved with the 30% porous-cell honeycomb installed compared to baseline results. The 30% porous-cell honeycomb also improved the results slightly over those obtained with the solid and 20% porous-cell honeycomb. By comparing the C_p values in the exit section in all orientations, the flow is fully uniform at L/D of 23.9.

4.2.3.4 40% Porous-Cell Honeycomb Pressure Results

Non-dimensional pressure distributions for the 40% porous-cell honeycomb installed after the 2nd elbow, along the duct for 3 azimuth angles of 0°, 180°, and 270° and for free-stream velocities of 60ft/s, 80ft/s, and 100ft/s are shown in Figures 4-28a, 4-28b, and 4-28c.

Pressure Results Along 0° Azimuth Angle

Measurements indicate, Figure 4-28a, that the C_p values are reduced in the exit duct compared to the baseline results when the 40% porous-cell honeycomb is installed. The flow in the exit section is more uniform; Sec 4.2.3.3. At the lower free-stream velocities tested, the values of C_p decrease further from those obtained with the 30% porous-cell honeycomb.

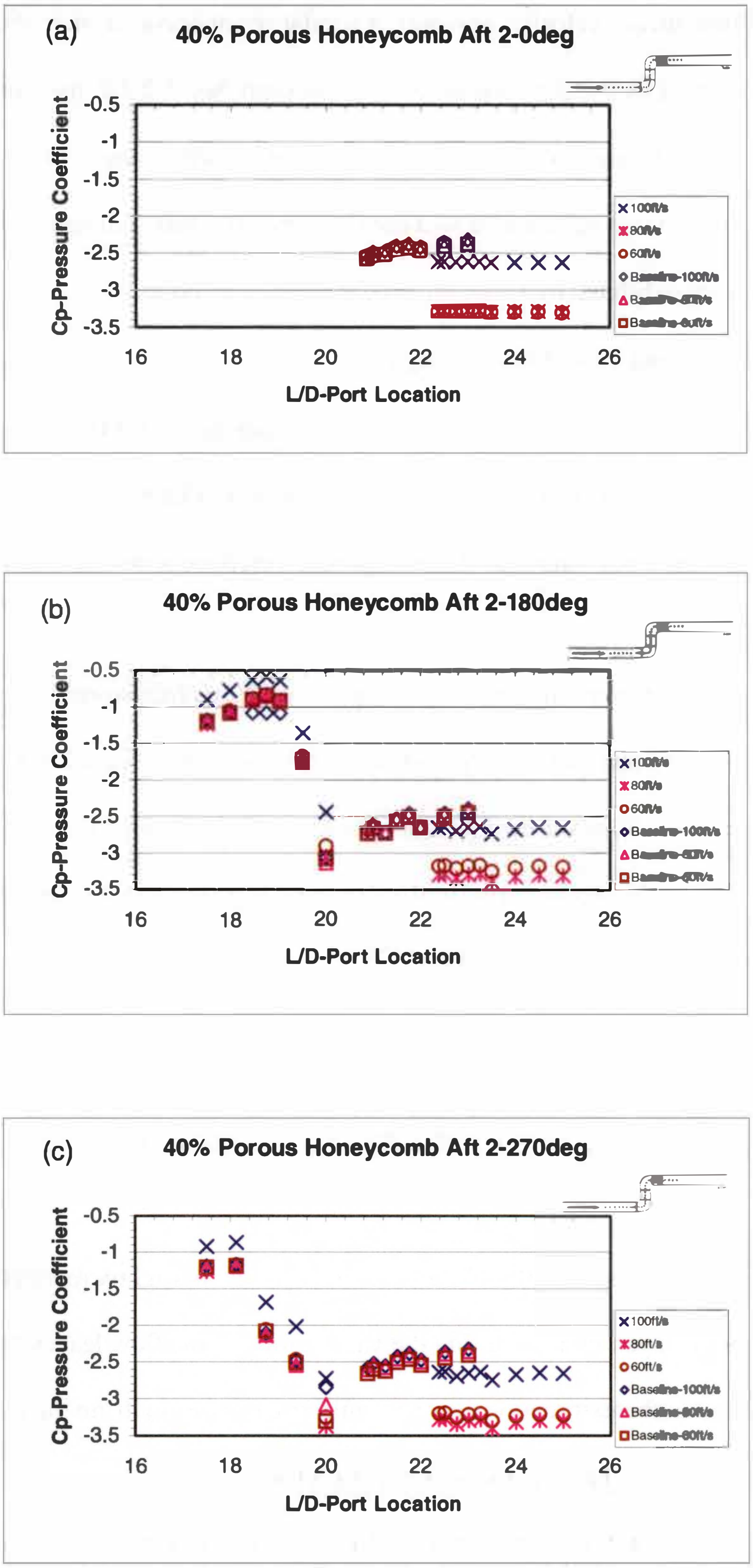

Figure 4-28. C_p vs. L/D-40% Porous-Cell Honeycomb Aft 2^{nd} Elbow

At the 100ft/s free-stream velocity, however, a similar result occurs as that obtained with 100ft/s free-stream velocity, 20% porous-cell honeycomb, Sec 4.2.3.2, the values of C_p increase from those obtained with the solid or 20% porous-cell honeycomb.

At all free-stream velocities tested the flow becomes fully uniform at L/D of 23.6. No more losses are exhibited by variations in C_p beyond this point.

Pressure Results Along 180° Azimuth Angle

Along the elbow, the 40% porous-cell honeycomb generates the highest values of C_p at the 100ft/s free-stream velocity than was previously seen, Figure 4-28b. At the lower free-stream velocities, the same values as the 30% porous-cell honeycomb are exhibited, Sec 4.2.3.3.

In the exit section of the duct, the C_p values at 100ft/s free-stream velocity are also higher than those obtained with the 30% porous-cell honeycomb, Sec 4.2.3.3. At the lower free-stream velocities, however the C_p values are lower than obtained with other honeycomb installed. The flow achieves uniform flow, recovering from the slight disturbances generated from the exit of the honeycomb at L/D of 23.7.

Pressure Results Along 270° Azimuth Angle

The trend exhibited in Figure 4-28c, is similar to that obtained with the 30% porous-cell honeycomb installed, Sec 4.2.3.3. The C_p values are slightly higher however, at the high free-stream velocity.

In the exit section, the 40% porous-cell honeycomb is slightly more effective than the 30% porous-cell honeycomb in lowering the values of C_p as the flow leaves the honeycomb section. The flow in the exit section becomes uniform, recovering from the losses generated when the flow leaves the honeycomb section, at L/D of 23.8.

The overall results obtained with the 40% porous-cell honeycomb installed showed improvements in lowering the C_p values in the exit section of the duct.

Overall, the results indicate that the honeycomb located after the 2nd elbow helps in redistributing the non-uniformities generated in the elbows. The porous-cell honeycomb helped to eliminate the axial disturbances in the flow while the non-porous sections performed the traditional role of eliminating the lateral disturbances. As a result, the flow leaving the honeycomb section and entering into the exit section of the duct had fewer losses and a higher local velocity than baseline values.

Figures 4-29(a-c) illustrate the average C_p in the exit section of the duct at all free-stream velocities tested. Since the flow in the exit duct is not fully uniform until C_p in each of the orientations is the same, these figures give a reasonable indication of the behavior of the flow as it leaves the honeycomb and travels through the exit duct. All the honeycombs exhibit significant improvement eliminating the disturbances in the flow and achieving a higher exit velocity.

The 40% porous-cell honeycomb lowered the C_p values in the exit section slightly more than the other honeycombs at the lower 2 free-stream velocities tested, however more disturbances and variations in C_p existed prior to the flow becoming fully uniform.

Figures 4-30(a-c) illustrate the average C_p in the exit duct for both sets of configurations. These figures indicate that overall the honeycomb after the 1st elbow establishes a slightly lower value of C_p, thus higher local velocity than the honeycomb after the 2nd elbow but does not become fully uniform until further downstream in the exit duct. The honeycomb after the 2nd elbow however, helps to establish a more uniform flow in a shorter distance downstream of the exit duct. Either configuration, however, significantly reduces the secondary flows generated by the curved duct.

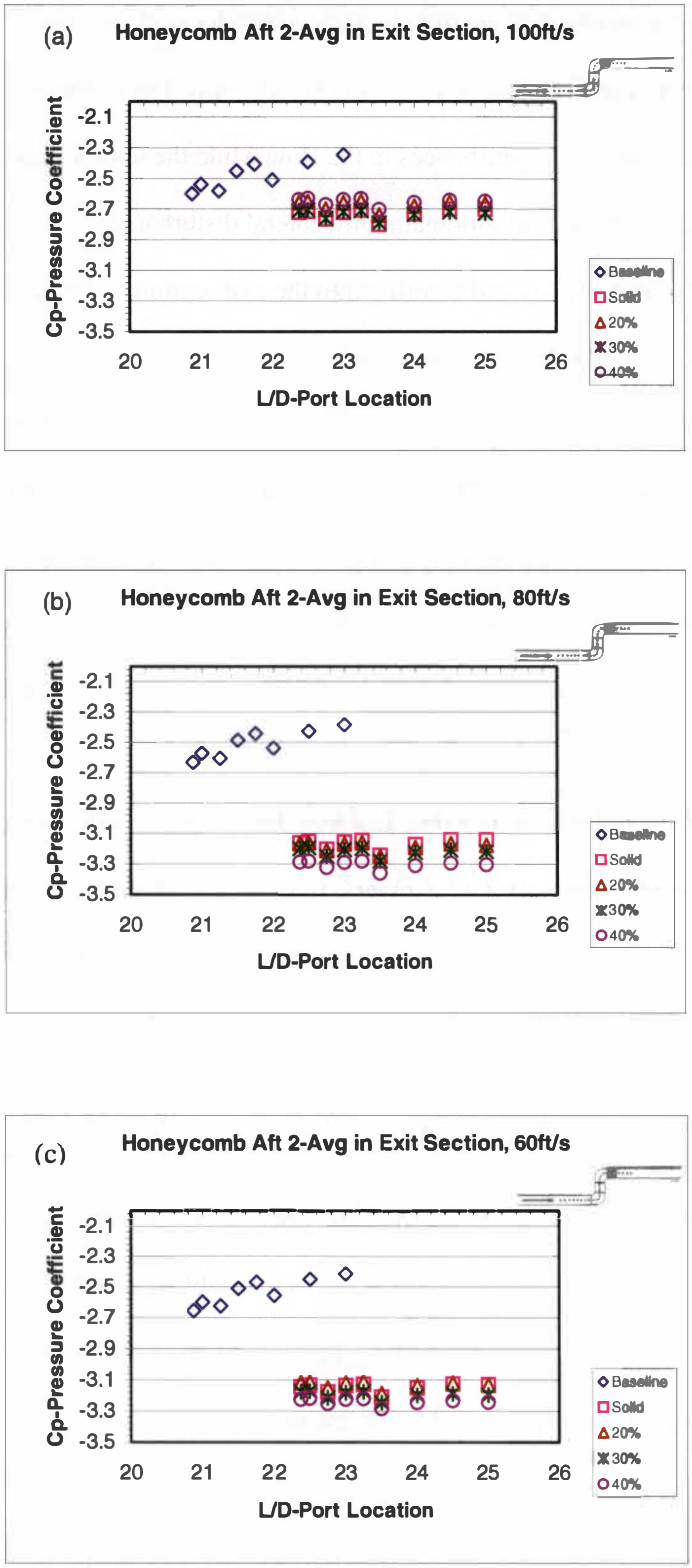

Figure 4-29. Honeycomb Aft 2nd Elbow, Average C_p in Exit Duct

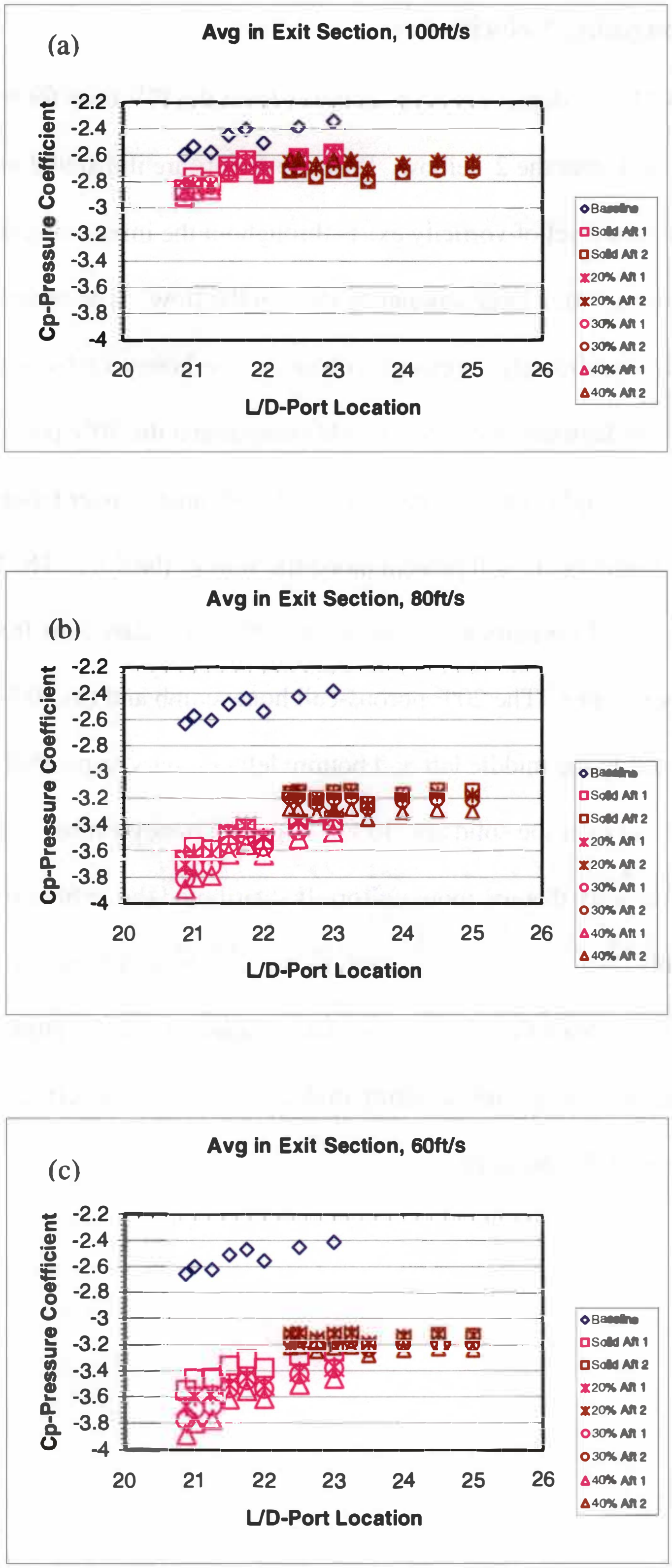

Figure 4-30. All Honeycombs, Average C_p in Exit Duct

4.3 Particle Imagining Velocimetry

Figures 4-31(a-e) depict vorticity contours from the PIV tests for baseline and for the honeycombs installed after the 2nd elbow. Baseline results are illustrated in the top left contour. A significant level of vorticity exists throughout the image indicating that the flow is highly non-uniform with a large amount of swirl in the flow. The other contours illustrate that flow quality is significantly improved with any of the honeycombs installed. Although the solid honeycomb depicted in the upper right contour and the 30% porous-cell honeycomb depicted in the middle right contour have improved flow quality over baseline, large concentrations of vorticity are still present along the wall of the duct. The larger concentration regions of vorticity are reminiscent of the secondary flow from the elbows, which are still in existence. The 20% porous-cell honeycomb and the 40% porous-cell honeycomb depicted in the middle left and bottom left contours respectfully, both show a definite improvement over the solid and 30% porous-cell honeycombs. They exhibit very small patches of vorticity that are more uniformly distributed throughout the flow. Smaller and more uniformly distributed areas of vorticity are the result of break-up and redistribution of the secondary flows from the two elbows. The smaller vorticity regions would dissipate more quickly, thus the honeycomb resulting in these cases are more effective towards controlling the flow at the duct exit.

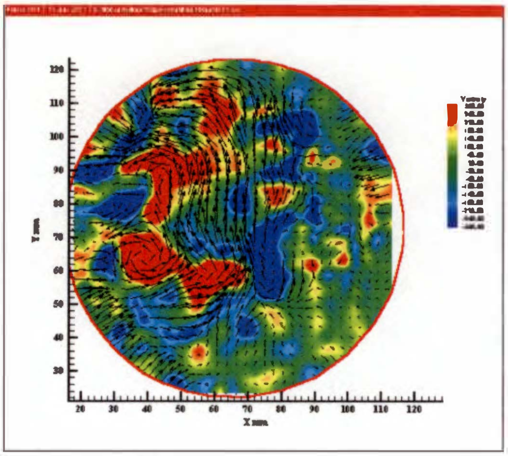

a. Baseline

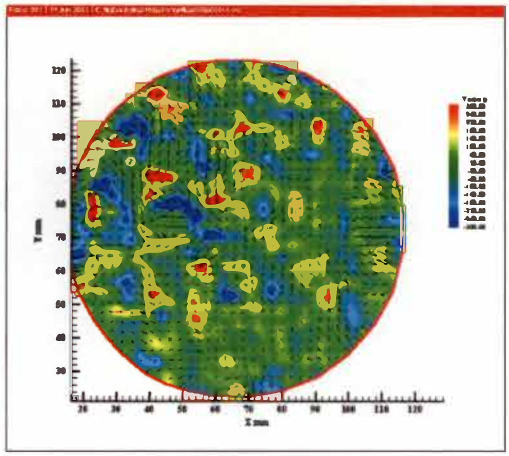

b. Solid Honeycomb

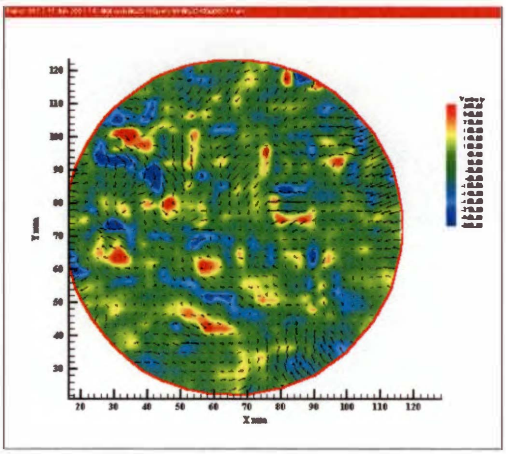

c. 20% Porous-cell Honeycomb

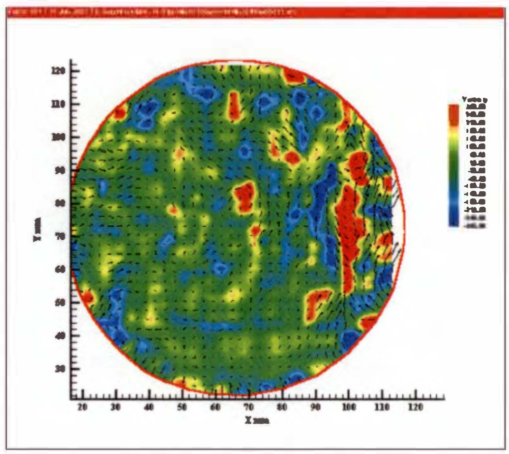

d. 30% Porous-cell Honeycomb

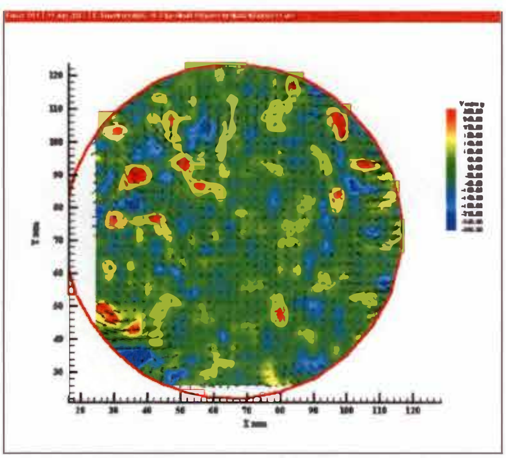

e. 40% Porous-cell Honeycomb

Figure 4-31. PIV Vorticity Contours

Chapter 5

Conclusions and Recommendations

An experimental study on the effectiveness of using honeycomb to improve flow quality in curved ducts by reducing secondary flow was conducted. Solid honeycomb and porous-cell honeycombs with varying porosity were installed at either of two locations, after the 1st elbow or after the 2nd elbow. The flow, particularly in the exit section of the duct, was analyzed using surface oil flow visualization, pressure measurements, and Particle Imaging Velocimetry (PIV) to determine if the secondary flows had diminished within a short distance downstream of the elbow with the honeycomb installed compared to the baseline flow.

The surface oil flow visualization provided a qualitative analysis of how the flow behaved in the exit section of the duct. The pressure measurements provided detail and qualitative insight on how the flow traveling through the elbows was affected by the different free-stream velocities. PIV was used to calculate the vorticity contours of each configuration, the contours helped to describe the secondary motion of the fluid at the exit section of the elbow. Based on this experimental study, the following conclusions are drawn:

- Higher free-stream velocities generate a larger region of separated and secondary flows in elbows.
- Locating the honeycomb after the 1st elbow eliminates more of the non-uniformities traveling into the 2nd elbow and into the exit section of the duct than either baseline or flow with a honeycomb after the 2nd elbow.
- Locating the honeycomb after the 2nd elbow generates a uniform flow within a shorter distance downstream of the elbow than the honeycomb located after the 1st elbow.

- PIV measurements agree with pressure measurements with respect to flow uniformity at the exit of the 2nd elbow.
- Porous-cell honeycomb is more effective than solid honeycomb at generating a uniform flow after an elbow.

Recommendations for future work include:

- Varying the total length of the honeycomb cell.
- Implementing more than one honeycomb or a combination of solid and porous-cell honeycombs in the duct.

List of References

References

1. Schlichting, H., "Boundary-Layer Theory", McGraw-Hill Book Company, 1968.
2. Wigeland, R.A., Ahmed, M., and Nagib, H.M., "Management of Swirling Flows with Application to Wind Tunnel Design", AIAA Journal, Vol. 16 No. 11, Nov 1978.
3. Scheiman, J. and Brooks, J.D., "Comparison of Experimental and Theoretical Turbulence Reduction from Screens, Honeycomb, and Honeycomb-Screen Combinations", AIAA Paper No. 80-0433R.
4. Furness, R., "Don't Install that Flow Meter", Flow Control Magazine, March 2002.
5. Vakili, A.D., University of Tennessee Space Institute, Professor.
6. Laws, E.M. and Chesnoy, A., "The Design and Development of Flow Conditioning Devices", FED Vol. 159, Devices for Flow Measurement and Control, ASME 1993, p11-18.
7. Vakili, A., and Wu, J.M., "Comparison of Experimental and Computational Compressible Flow in an S-Duct", AIAA Paper No. 84-0033, Reno NV, Jan 1984.
8. Robertson, J.A. and Crowe, C.T., "Engineering Fluid Mechanics, Sixth Edition", John Wiley and Sons Inc, 1997.
9. Vakili, A.D., Wu, J.M., Liver, P., and Bhat, M.K., "Flow Control in a Diffusing S-Duct", AIAA Paper No. 85-0524, Boulder CO, Mar 1985.
10. Reichert, B.A. and Wendt, B.J., "Improving Diffusing S-Duct Performance by Secondary Flow Control", AIAA Paper No. 99-0739, Reno NV, Jan 1994.
11. Anabtawi, A.J., Blackwelder, R.F., Lissaman, P.B.S., and Liebeck, R.H., "An Experimental Investigation of Boundary Layer Ingestion in a Diffusing S-Duct with and Without Passive Flow Control", AIAA Paper No. 99-0739, Reno NV, Jan 1999.

12. Jenkins, L., Gorton, S.A., and Anders, S., "Flow Control Device Evaluation for an Internal Flow with Adverse Pressure Gradient", AIAA Paper No. 2002-0266, Reno NV, Jan 2002.
13. Farell, C., Saxena, V., and Youssef, S., "Experiments on Turbulence Management Using Screens and Honeycombs", FED-159, Devices for Flow Measurement and Control, ASME p1-10, 1993.
14. Dryden, H.L. and Schubauer, G.B., "The Use of Damping Screens for the Reduction of Wind-Tunnel Turbulence", Journal of Aeronautical Sciences, Apr 1947, p221-228.
15. Elder III, E.C., "A Comparative Experimental Study of Turbulence Reduction by Porous Honeycomb-A First Look", University of Tennessee Master's Thesis, Aug 2001.
16. Lumley, J.L., "Passage of a Turbulent Stream Through Honeycomb of Large Length-to-Diameter Ratio", Transactions of the ASME, June 1964, p218-220.
17. Loehrke, R.I. and Nagib, H.M., "Control of Free-Stream Turbulence by Means of Honeycombs: A Balance Between Suppression and Generation", Transactions of the ASME, Journal of Fluids Engineering, Sep 1976, p342-353.
18. Munson, B.R., Young, D.F., and Okiishi, T.H., "Fundamentals of Fluid Mechanics", John Wiley and Son Inc, 1990.
19. Rosemount Product Data Sheet 2256, "Model 1151DP Alphaline Differential Pressure Transmitter", Rosemount Inc
20. www.science.widener.edu
21. Rabinovich, S., "Measurement Errors: Theory and Practice", American Institute of Physics, 1995.

Appendices

Appendix A

Error Analysis

The errors of each of the contributing variables must be considered as they propagate through the experimental procedure to determine the error band on the non-dimensional pressure distribution, C_p.

$$C_p = f(P, \rho, U_\infty),$$

P = pressure, ρ = density, and U_∞ = free-stream velocity.

The density was obtained from the ideal gas law, with the known pressure and temperature at the first port location.

$$\rho = f(P, T),$$

T = temperature.

Once the density was determined, the free-stream velocity at the first port was obtained from Bernoulli's equation.

The averaged pressure, temperature, density, velocity, and change in pressure at the first port location are:

$P = 5.989 inH_2O$

$T = 70.47F$

$\rho = 0.002281 slugs/ft^3$

$U_\infty = 100 ft/s$

$\Delta P = 2.239 inH_2O$

Known errors are:

$T = \pm 2F$

$P = \pm 0.25\% = 0.011 inH_2O$

Using the following equations [20, 21], error propagation through the experimental procedure was determined:

Addition:	$x = a + b;$	$S_x = \sqrt{}(S_a^2 + S_b^2 + S_c^2$
Multiplication/Division:	$x = a*b/c$	$S_x = x*\sqrt{}(S_a/a)^2 + (S_b/b)^2 + (S_c/c)^2$
Exponential:	$x = a^b$	$S_x = x*b*(S_a/a)$

Where x = result of calculation;

S_x = error in result;

a, b, and c are values of variables; and

S_a, S_b, and S_c are error in variables.

These equations yielded the following errors:

$\rho_{error} = \pm 6.5E\text{-}4 slugs/ft^3$

$\Delta P_{error} = \pm 0.01556 inH_2O$

$V_{error} = \pm 1.47 ft/s$

$C_{perror} = \pm 0.085$

The error band for the non-dimensional pressure distributions is ± 0.085.

Appendix B

Pressure Measurement Port Location

Pressure measurements as detailed in Sec 3.3.1 are located longitudinally along the duct for 3 azimuth angles: 0°, 180°, and 270°. Figure B1-1 illustrates the duct geometry and shows locations of the ports. Table B1-1 provides details on location of the pressure port from the inlet of the duct, as well as the non-dimensional port location. Table B1-1 also details which region of the duct the pressure port is located and at which azimuth angle it was obtained.

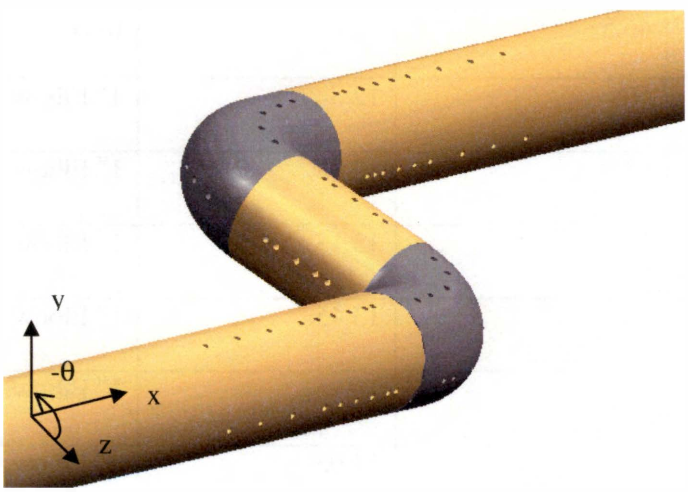

Figure B1-1. Pressure Port Locations Along the Duct

Table B1-1. Pressure Port Details

Port Number	Location from Inlet (inches)	Non-Dimensional Port Location	Duct	Azimuth Angle
1	0	0	Inlet	0°, 180°, 270°
2	36	9	Inlet	0°, 180°, 270°
3	38	9.5	Inlet	0°, 180°, 270°
4	40	10	Inlet	0°, 180°, 270°
5	42	10.5	Inlet	0°, 180°, 270°
6	43	10.75	Inlet	0°, 180°, 270°
7	44	11	Inlet	0°, 180°, 270°
8	45	11.25	Inlet	0°, 180°, 270°
9	46	11.5	Inlet	0°, 180°, 270°
10	46.5	11.63	Inlet	0°, 180°, 270°
11	50	12.5	1st Elbow	0°, 270°
12	51.9	12.98	1st Elbow	270°
13	52.5	13.13	1st Elbow	0°
14	53.8	13.45	1st Elbow	270°
15	55	13.75	1st Elbow	0°, 270°
16	56.2	14.05	1st Elbow	270°
17	57.5	14.38	1st Elbow	0°
18	58.1	14.53	1st Elbow	270°
19	60	15	1st Elbow	0°, 270°
20	63.5	15.88	6-in connector	0°, 180°, 270°
21	64	16	6-in connector	0°, 180°, 270°

Table B1-1. Cont'd

Port Number	Location from Inlet (inches)	Non-Dimensional Port Location	Duct	Azimuth Angle
22	65	16.25	6-in connector	0°, 180°, 270°
23	66	16.5	6-in connector	0°, 180°, 270°
24	66.5	16.63	6-in connector	0°, 180°, 270°
25	70	17.5	2nd elbow	180°, 270°
26	71.9	17.98	2nd elbow	270°
27	72.5	18.13	2nd elbow	180°
28	73.8	18.45	2nd elbow	270°
29	75	18.75	2nd elbow	180°, 270°
30	76.2	19.05	2nd elbow	270°
31	77.5	19.38	2nd elbow	180°
32	78.1	19.53	2nd elbow	270°
33	80	20	2nd elbow	180°, 270°
34	83.5	20.88	Exit	0°, 180°, 270°
35	84	21	Exit	0°, 180°, 270°
36	85	21.25	Exit	0°, 180°, 270°
37	86	21.5	Exit	0°, 180°, 270°
38	87	21.75	Exit	0°, 180°, 270°
39	88	22	Exit	0°, 180°, 270°
40	90	22.5	Exit	0°, 180°, 270°
41	92	23	Exit	0°, 180°, 270°
42	94	23.5	Exit	0°, 180°, 270°

Vita

Michelle Yvonne Vella was born on 7th October 1972 in Etobicoke, Ontario Canada. After graduating in June 1991 from Holy Name of Mary High School in Mississauga, Ontario, she joined the Canadian Armed Forces. Upon completion of the Basic Officer Training Course in Chilliwack, British Columbia, she attended the Royal Military College of Canada in Kingston, Ontario and graduated in May 1995 with a Bachelor's Degree in Mechanical Engineering. After completing occupational training as an Aerospace Engineering Officer in Borden, Ontario, Lieutenant Vella was posted to Ottawa, Ontario in the Directorate Intelligence and Security Operations Automation where she was responsible for the Information Technology Systems of the Military Police and Special Investigations Unit. While in Ottawa she also worked as a Project Officer in the Chief Information Office of the Vice Chief of the Defense Staff. In July 1999, Captain Vella was posted to the Aerospace and Telecommunications Engineering Support Squadron (ATESS) in Trenton, Ontario where she worked as an Aircraft Structural Projects Officer. During her time at ATESS, she became the section leader of the Aircraft Structural Projects Section. In 2001, Captain Vella was selected by the Canadian Forces for post-graduate training at the University of Tennessee Space Institute where she completed her Masters of Science Degree in Aerospace Engineering in August 2003. Captain Vella is posted back to Ottawa, Ontario Canada where she will work in the Directorate of Technical Airworthiness as an Aerospace Certification Engineer.

7811 0207 53
11/05/03 MAB